Cu^II Complexes and Coordination Polymers with Pyridine or Pyrazine Amides and Amino Benzamides—Structures and EPR Patterns

Ines Wackerbarth [1], Ni Nyoman Agnes Tri Widhyadnyani [1], Simon Schmitz [1], Kathrin Stirnat [1], Katharina Butsch [1], Ingo Pantenburg [1], Gerd Meyer [1,2] (ID) **and Axel Klein [1,*]** (ID)

[1] Department für Chemie, Institut für Anorganische Chemie, Universität zu Köln, Greinstrasse 6, D-50939 Köln, Germany; ines.wackerbarth@gmail.com (I.W.); widhyadnyani.agnes@gmail.com (N.N.A.T.W.); s.schmitz@uni-koeln.de (S.S.); kstirnat@gmail.com (K.S.); Katharinabutsch@web.de (K.B.); ac118@uni-koeln.de (I.P.); gerdm@kth.se (G.M.)

[2] Department of Chemistry, KTH Royal Institute of Technology, Teknikringen 30, SE-100 44 Stockholm, Sweden

* Correspondence: axel.klein@uni-koeln.de; Tel.: +49-221-470-4006

check for updates

Abstract: Isonicotine amide, picoline amide, pyrazine 2-amide, 2- and 4-amino benzamides and various Cu^II salts were used to target Cu^II complexes of these ligands alongside with 1D and 2D coordination polymers. Under the criterion of obtaining crystalline and single phased materials a number of new compounds were reliably reproduced. Remarkably, for some of these compounds the ideal Cu:ligand ratio of the starting materials turned out to be very different from Cu:ligand ratio in the products. Crystal and molecular structures from single-crystal XRD were obtained for all new compounds; phase purity was checked using powder XRD. We observed exclusively the O_{amide} and not the NH_{2amide} function binding to Cu^II. In most of the cases; this occurred in chelates with the second pyridine, pyrazine or aminophenyl N function. μ-*O,N* ditopic bridging was frequently observed for the N = pyridine, pyrazine or aminophenyl functions, but not exclusively. The geometry around Cu^II in these compounds was very often axially elongated octahedral or square pyramidal. X-band EPR spectra of powder samples revealed various spectral symmetry patterns ranging from axial over rhombic to inverse axial. Although the EPR spectra cannot be unequivocally correlated to the observed geometry of Cu^II in the solid state structures, the EPR patterns can help to support assumed structures as shown for the compound [Cu(Ina)_2Br_2] (Ina = isonicotine amide). As UV-vis absorption spectroscopy and magnetic measurement in the solid can also be roughly correlated to the surrounding of Cu^II, we suggest the combination of EPR, UV-vis spectroscopy and magnetic measurements to elucidate possible structures of Cu^II compounds with such ligands.

1. Introduction

Pyridine carboxamides, pyrazine carboxamides and amino-benzamides (Scheme 1) are interesting ditopic ligands for Cu^II coordination chemistry [1–32]. One reason is their use as versatile building blocks in coordination polymers and MOFs for various applications [1–3,8,9,11–13,16,20,21,26,27]. Another important reason is the biological relevance of some of the ligands used in this study (Scheme 1) [4–6,17,18,24,33]. An interesting general aspect of these ligands is the preference of Cu^II to the different (offered) donor atoms in the ligands. From the viewpoint of the HSAB principle the N atom of the heteroaromatic cores is softer than the amine function of 4-amino benzamide and both are softer than the O amide function of amides or corresponding carboxylates. From the viewpoint of Cu metalloenzymes the frequent binding of soft ligands such as histidine-*N* and cysteine-*S* confirms the

tendency of Cu to softer ligands [33]. However, in various Cu enzymes also harder donor functions such as carboxylates were coordinated [34,35]. In metalloenzymes, carboxylate side chains of the peptide are very frequent ligands and were preferably coordinated by hard metal ions, as expected. In contrast to this, carboxamide side chains were less preferred as ligands in metalloenzymes [34–36], in agreement with the observation that the carboxamide function coordinates only effectively in chelate ligands as 2-pyridine or 2-pyrazine carboxamides [1–3,5,6,15–20,22–26,32,37–41].
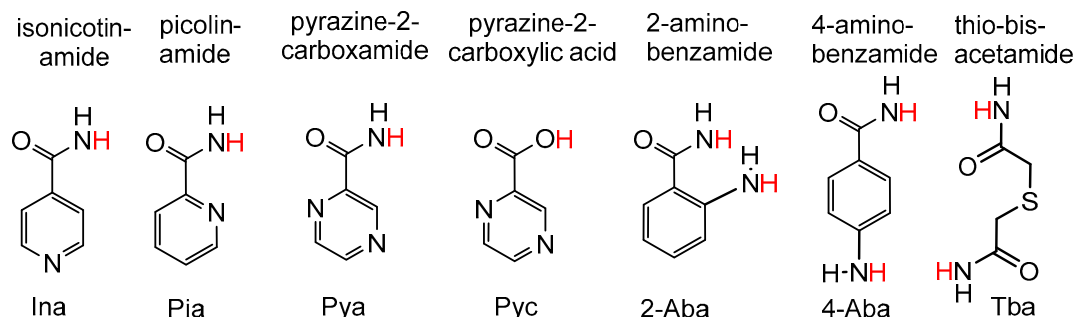
Scheme 1. Protoligands (ligand precursor prior to deprotonation) with abbreviations used in this study. In red: acidic protons.

Herein we report on a study aiming to explore the binding preferences of isonicotinamide (Ina), picolinamide (Pia), pyrazine-2-carboxamide (Pya) and 2- and 4-amino-benzamides (2- and 4-Aba; Scheme 1) towards Cu^{II}. We also added the versatile ligand thio-bisacetamide (Tba) to this study, as Tba represents the aliphatic amides and we expected that the ligand will form $S\hat{}O$ or $S\hat{}N$ chelates. The ligands were reacted with various Cu^{II} salts in EtOH without addition of bases to avoid deprotonation of the ligands. The compounds produced were studied in the solid state by single crystal and powder X-ray diffraction, EPR, magnetic measurements and UV-vis absorption spectroscopy. Being aware of the problem that our so-called "combinatorial approach"—which means dissolving metal salts and ligands and crystallising materials out of the mixture—might lead to a plethora of different structures, we aimed to work out reliable procedures for the preparation of defined structures which also allow reproducing the materials. We succeeded in doing so in many cases, and powder X-ray diffraction (PXRD) was used to evaluate the preparation methods and to prove the phase purity of the compounds. This also means that non-crystalline materials and materials which obviously contained mixtures of compounds as could be seen from their colours, which were obtained from further reactions of the seven ligands and the Cu salts, were not further analysed. Interestingly, this comprises all trials using nicotinamide as ligand.

Special focus was also laid on EPR spectroscopy of these solids. Having so many new structures and EPR data in hand we were able to correlate details in the EPR spectra such as spectral symmetry and *g* values to the local environment of the Cu^{II} centres. Magnetic and UV-vis absorption data of selected samples were also recorded.

2. Results and Discussion

2.1. Synthesis of the Cu Complexes

In a first series of experiments Cu^{II} salts were reacted with the ligands shown in Scheme 1 in a Cu:ligand ratio of 1:1 in EtOH. Single crystals of 18 compounds were obtained by slow evaporation of the solvent from the reaction mixtures (Table 1). The Cu:ligand ratios were found ranging from 1:1 to 1:4. Coligands to Cu^{II} were the anions from the Cu sources: Cl^-, Br^-, NO_3^-, BF_4^-, Tfa^-, EtOH and H_2O. ClO_4^- was not coordinating but found as a counter ion. None of the ligands was found deprotonated in the structures. However, pyrazine-2-carboxamide was converted into pyrazine carboxylate forming the compound [Cu(Pyc)(Tfa)](**11**) in neutral aqueous EtOH solution. In HCl acidic solutions isonicotinamide (Ina) was protonated yielding $(HIna)_2[CuCl_4]\cdot 2H_2O$ (**6**)

and (HIna)[Cu(H$_2$O)Cl$_3$] (**7**) both containing 4-carboxamidopyridin-1-ium (HIna$^+$) cations. Under similar conditions 4-aminobenzamide was protonated to 4-benzamidyl-ammonium (4-AbaH$^+$) in [Cu(4-HAba)$_2$Cl$_4$] (**17**). A very interesting finding was that the complex [Cu(Ina)$_2$(NO$_3$)$_2$] (**2**) could be converted into [Cu(Ina)$_2$Br$_2$] (**5**) through grinding with KBr. Unfortunately, the obtained crystals of this compound were of poor quality preventing a structure solution. In a previous report of (**5**) space group *P*2$_1$/c (No. 14) was concluded from 24 reflections by powder XRD and the authors assumed a polymeric structure with a distorted octahedral coordination around Cu^{II} [39]. From the new compound [Cu(Ina)$_4$(H$_2$O)$_2$](BF$_4$)$_2$ (**1**), the crystal structure of the corresponding ClO$_4$$^-$ salt was previously reported alongside with the structure of [Cu(Ina)$_2$(H$_2$O)$_2$(NO$_3$)$_2$] (**3**) [16]. All other crystal structures are new (see Figures S1–S40 and full data in Tables S1–S39 in the Supplementary Materials).

Table 1. Overview over the obtained crystalline compounds and structures.

Ligand	Cu^{II} Precursor	Compound	Formula (Weight)	Space Group
Ina	Cu(BF$_4$)$_2$·6H$_2$O	[Cu(Ina)$_4$(H$_2$O)$_2$](BF$_4$)$_2$ (**1**)	C$_{24}$H$_{28}$B$_2$Cu$_1$F$_8$N$_8$O$_6$ (761.69)	*C*2/c (No. 15) [d]
Ina	Cu(NO$_3$)$_2$·3H$_2$O	$^1_\infty$[Cu(Ina)$_2$(NO$_3$)$_2$] (**2**)	C$_{12}$H$_{12}$Cu$_1$N$_6$O$_8$ (431.81)	*P*2$_1$2$_1$2$_1$ (No. 19)
Ina	Cu(NO$_3$)$_2$·3H$_2$O	[Cu(Ina)$_2$(H$_2$O)$_2$(NO$_3$)$_2$] (**3**)	C$_{12}$H$_{16}$Cu$_1$N$_6$O$_{10}$ (467.84)	*P*2$_1$/c (No. 14) [e]
Ina	Cu(BF$_4$)$_2$·6H$_2$O	[Cu(Ina)$_2$(H$_2$O)$_3$(SiF$_6$)]·H$_2$O (**4**)	C$_{12}$H$_{20}$Cu$_1$F$_6$N$_4$O$_6$Si$_1$ (521.94)	*P*-1 (No. 2)
Ina	[Cu(Ina)$_2$(NO$_3$)$_2$]	[Cu(Ina)$_2$Br$_2$] (**5**)	C$_{12}$H$_{12}$Br$_2$Cu$_1$N$_4$O$_2$ (467.61)	*P*2$_1$ (No. 4) [f]
HIna$^+$ [a]	CuCl$_2$·2H$_2$O	(HIna)$_2$[CuCl$_4$]·2H$_2$O (**6**)	C$_{12}$H$_{18}$Cl$_4$CuN$_4$O$_4$ (487.64)	*P*-1 (No. 2)
HIna$^+$ [a]	CuCl$_2$·2H$_2$O	(HIna)[Cu(H$_2$O)Cl$_3$] (**7**)	C$_6$H$_9$Cl$_3$Cu$_1$N$_2$O$_2$ (311.05)	*P*-1 (No. 2)
Pia	Cu(BF$_4$)$_2$·6H$_2$O	[Cu(Pia)$_2$(BF$_4$)$_2$] (**8**)	C$_{12}$H$_{12}$B$_2$Cu$_1$F$_8$N$_4$O$_2$ (481.41)	*P*-1 (No. 2)
Pya	Cu(BF$_4$)$_2$·6H$_2$O	$^2_\infty$[Cu(Pya)$_2$](BF$_4$)$_2$ (**9**)	C$_{10}$H$_{10}$B$_2$Cu$_1$F$_8$N$_6$O$_2$ (483.38)	*P*2$_1$/c (No. 14)
Pya	Cu(NO$_3$)$_2$·3H$_2$O	[Cu(Pya)$_2$(H$_2$O)(NO$_3$)](NO$_3$) (**10**)	C$_{10}$H$_{12}$Cu$_1$N$_8$O$_9$ (451.80)	*P*-1 (No. 2)
Pya	Cu(NO$_3$)$_2$·3H$_2$O	$^1_\infty$[Cu(Pya)(NO$_3$)$_2$] (**11**)	C$_5$H$_5$Cu$_1$N$_5$O$_7$ (310.67)	*C*2/c (No. 15)
Pyc$^-$ [b]	Cu(Tfa)$_2$·H$_2$O	$^2_\infty$[Cu(Pyc)(Tfa)] (**12**)	C$_7$H$_3$Cu$_1$F$_3$N$_2$O$_4$ (299.65)	*P*2$_1$2$_1$2$_1$ (No. 19)
2-Aba	Cu(NO$_3$)$_2$·3H$_2$O	[Cu(2-Aba)$_2$(NO$_3$)$_2$] (**13**)	C$_{14}$H$_{16}$Cu$_1$N$_6$O$_8$ (459.86)	*P*2$_1$/n (No. 14) [g]
4-Aba	Cu(NO$_3$)$_2$·3H$_2$O	$^1_\infty$[Cu$_2$(4-Aba)$_2$(H$_2$O)$_3$(NO$_3$)$_3$](NO$_3$) (**14**)	C$_{14}$H$_{22}$Cu$_2$N$_8$O$_{17}$ (701.46)	*C*2/c (No. 15) [h]
4-Aba	Cu(ClO$_4$)$_2$·6H$_2$O	$^2_\infty$[Cu(4-Aba)$_2$(EtOH)$_2$](ClO$_4$)$_2$ (**15**)	C$_{18}$H$_{28}$Cl$_2$Cu$_1$N$_4$O$_{12}$ (626.88)	*P*2$_1$/c (No. 14)
4-Aba	Cu(BF$_4$)$_2$·6H$_2$O	$^2_\infty$[Cu(4-Aba)$_2$(EtOH)$_2$](BF$_4$)$_2$ (**16**)	C$_{18}$H$_{28}$B$_2$Cu$_1$F$_8$N$_4$O$_4$ (601.60)	*P*2$_1$/c (No. 14)
4-HAba$^+$ [c]	Cu(ClO$_4$)$_2$·6H$_2$O + HCl	[Cu(4-HAba)$_2$Cl$_4$] (**17**)	C$_{14}$H$_{18}$Cl$_4$Cu$_1$N$_4$O$_2$ (479.67)	*P*2$_1$/c (No. 14)
Tba	Cu(ClO$_4$)$_2$·6H$_2$O	[Cu(Tba)$_2$](ClO$_4$)$_2$ (**18**)	C$_8$H$_{16}$Cl$_2$Cu$_1$N$_4$O$_{12}$S$_2$ (558.80)	*C*2/m (No. 12)

[a] HIna$^+$ = 4-carboxamidopyridin-1-ium. [b] Pyc$^-$ = pyrazine-2-carboxylate. Tfa$^-$ = trifluoroacetate. [c] 4-AbaH$^+$ = 4-benzamidyl ammonium. [d] The ClO$_4$-salt was reported in *C*2/c previously, [16]. [e] Reported previously, [16]. [f] No valid structure refinement possible; previous assignment from powder XRD = *P*2$_1$/c (No. 14), from [22]. [g] A refinement in the standard space group *P*2$_1$/c was not successful. [h] The structure could not be fully refined: The nitrate anions around the N2 (coordinating) and N3 (non-coordinating) atoms show systematic disorder due to symmetric alternation. For the coordinating N2-nitrate there are two possible symmetric identical positions to bridge between the two Cu1 ions, both with an occupation of 0.5. This leads to two nitrate anions in very close proximity in the cell, but must be understood as alternating motif in consecutive cells. The non-coordinating nitrate N3 atom shows similar disorder (for details, see Tables S30 and S31).

In a further series of experiments, we tried to reproduce the obtained compounds and optimise their yields. Cl and Br turned out to be very strong ligands to Cu^{II} compared with the amides and we avoided them in these experiments. Similar observations that Cu–halide bonding dominates the structures of heteroleptic halide pyridine-amide Cu^{II} complexes were reported before [3,5,25–27,38,40]. Using the same reaction protocol but varying the Cu:ligand ratio, 10 out of these 18 compounds could be reliably reproduced in good to excellent yields and high phase purity as confirmed through elemental analyses and powder XRD (Scheme 2). In turn, this means that the compounds **2**, **4**, **11**, and **14** remained unreproducible.

Cu:ligand

Compound		3:1	2:1	1:1	1:2	1:3
$[Cu(Ina)_4(H_2O)_2](BF_4)_2$	(**1**)	3:1	2:1	1:1	1:2	1:3
$[Cu(Ina)_2(H_2O)_2(NO_3)_2]$	(**3**)	3:1	2:1	1:1	1:2	1:3
$[Cu(Pia)_2(BF_4)_2]$	(**8**)	3:1	2:1	1:1	1:2	1:3
$[Cu(Pya)_2(H_2O)(NO_3)](NO_3)$	(**10**)	3:1	2:1	1:1	1:2	1:3
$[Cu(Pya)_2](BF_4)_2$	(**9**)	3:1	2:1	1:1	1:2	1:3
$[Cu(Pyc)(Tfa)]$	(**12**)	3:1	2:1	1:1	1:2	1:3
$[Cu(2\text{-}Aba)_2(NO_3)_2]$	(**13**)	3:1	2:1	1:1	1:2	1:3
$[Cu(4\text{-}Aba)_2(EtOH)_2](ClO_4)_2$	(**15**)	3:1	2:1	1:1	1:2	1:3
$[Cu(4\text{-}Aba)_2(EtOH)_2](BF_4)_2$	(**16**)	3:1	2:1	1:1	1:2	1:3
$[Cu(Tba)_2](ClO_4)_2$	(**18**)	3:1	2:1	1:1	1:2	1:3

Scheme 2. Results of reproduction and optimisation reactions with yields and purities decreasing along the colour series: ▮▮▮▮. Yields were defined relative to the ligands (for details, see Experimental Section).

For some of the compounds such as $[Cu(Tba)_2](ClO_4)_2$ (**18**), $[Cu(4\text{-}Aba)_2(EtOH)_2](BF_4)_2$ (**16**), $[Cu(Pya)_2](BF_4)_2$ (**9**), and $[Cu(2\text{-}Aba)_2(NO_3)_2]$ (**13**), the optimum Cu:ligand ratio was the same as the stoichiometry of the compound. Remarkably, this is also true for $[Cu(Pyc)(Tfa)]$ (**12**) which was produced from a 1:1 mixture of $Cu(Tfa)_2 \cdot H_2O$ and pyrazine-amide (Pya).

For other compounds, the optimum ratio lies more to the Cu side with the most remarkable example being $[Cu(Ina)_4(H_2O)_2](BF_4)_2$ (**1**) for which a 2:1 = Cu:ligand ratio was best to observe phase pure material, while a 1:4 ratio prevails in the compound. The most important parameter for the assessment of the synthesis was the phase purity. The second important parameter was the yield. However, it is important to note, that yields were either calculated based on Cu or based on the ligand. For example, for compound (**1**) a 2:1 ratio in the starting material meant a high yield relative to the ligand (88%) but, of course, a very low yield relative to the starting Cu^{II} precursor (22%).

IR spectroscopy allowed revealing some structural features of the compounds (data in the Experimental Section). The presence of BF_4^-, ClO_4^-, and NO_3^- in the compounds as ligands or as counter anions is easily detectable through their characteristic vibrational modes. On the other hand, the data did not unequivocally allow determining whether these anions are ligands or counter ions. For example, in $[Cu(Ina)_4(H_2O)_2](BF_4)_2$ (**1**) the $\nu(B\text{–}F)$ vibration is found as a strong band at 1080 cm^{-1}, but as very strong broad resonance at 1050 cm^{-1} for $[Cu(Pya)_2](BF_4)_2$ (**9**). Both structures contain BF_4^- as counter anion. The complex $[Cu(Pia)_2(BF_4)_2]$ (**8**) contains two BF_4 ligands and the $\nu(B\text{–}F)$ is found at 1072 cm^{-1} as a strong band. Furthermore, for $[Cu(Ina)_2(NO_3)_2]$ (**2**) the $\nu(NO_3^-)$ resonance is observed at 1383 cm^{-1}, but is shifted to 1283 cm^{-1} for $[Cu(Pya)(NO_3)_2]$ (**11**) although both contain NO_3^- ligands. Additionally, for $[Cu(Pya)_2(H_2O)(NO_3)](NO_3)$ (**10**) only one $\nu(NO_3^-)$ vibration is found at 1350 cm^{-1} although one NO_3^- is coordinated, while the other serves as counter ion.

Quite generally, the coordination to Cu leads to slight blue-shifts of characteristic ligand vibrations. However, there are exceptions like the compounds containing pyrazine 2-amide (Pya). The $\nu(C=O)$ resonances for the compounds were found markedly at lower energy compared with those of the uncoordinated ligand. Interestingly, the $\delta(NH_2)$ resonances of the amide ligands are usually red-shifted upon coordination and suffer from a marked loss of intensity. However, in none of our structures did the NH_{2amide} function act as coordinating (see next paragraph). Thus, IR spectroscopy does not allow the unequivocal assignment of structural details.

2.2. Crystal Structures from Single Crystal XRD

The compounds listed in Table 1 could be obtained as single crystals suitable for single-crystal XRD directly from the reaction mixtures. Amongst the structures we found the 1D coordination polymers **2** (Figure 1), **11** (Figure 2), and **14** (Figure S29, Supplementary) and the 2D coordination polymers **9** (Figure 3), **12** (Figure S23), **15** (Figure S31), and **16** (Figure S34) in which the ditopic ligands isonicotine (Ina), pyrazine 2-amide (Pya), and 4-amino benzamide (4-Aba) bridge between Cu^{II} centres. Importantly, Ina, Pya and 4-Aba use the O_{amide} exclusively and not the NH_{2amide} function for the μ-*O,N* ditopic bridging with *N* = pyridine, pyrazine, or aminophenyl functions.
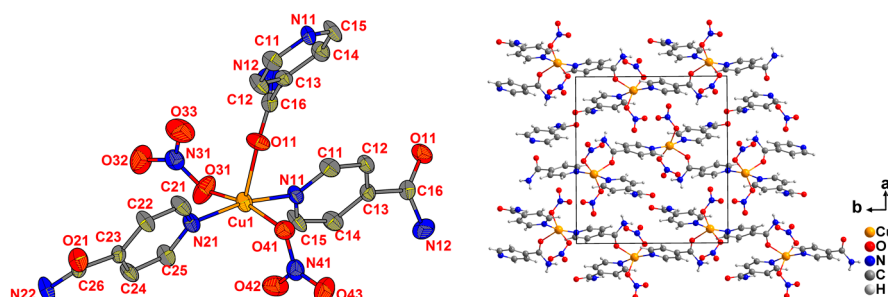

Figure 1. ORTEP representation (50% probability level) of the molecular entity within the structure of $^{1}_{\infty}$[Cu(Ina)$_2$(NO$_3$)$_2$] (**2**) (**left**); packing along the *c* axis in the crystal (**right**); H atoms were omitted for clarity.
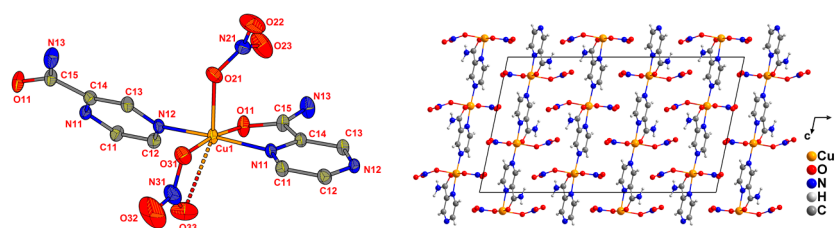
Figure 2. ORTEP representation (50% probability level) of the molecular entity within the structure of $^{1}_{\infty}$[Cu(Pya)(NO$_3$)$_2$] (**11**) (**left**); packing along the *b* axis in the crystal (**right**); H atoms were omitted for clarity.
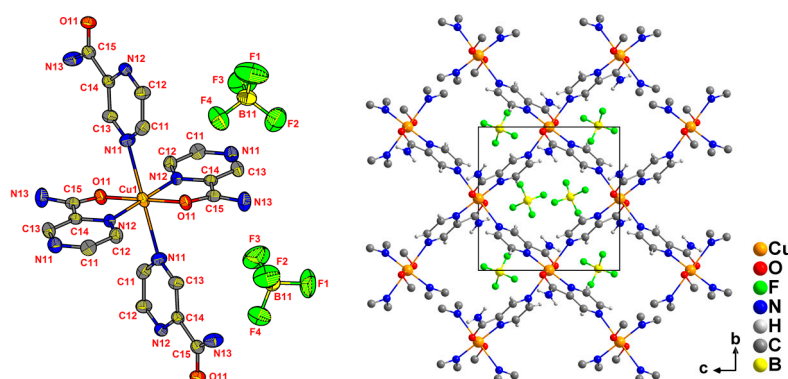

Figure 3. ORTEP representation (50% probability level) of the molecular entity within the structure of $^{2}_{\infty}$[Cu(Pya)$_2$](BF$_4$)$_2$ (**9**) (**left**); packing along the *a* axis in the crystal (**right**); H atoms were omitted for clarity.

At the same time, Pia, Pya, and 2-Aba form κ^2-*N,O*-chelates with Cu in **8** (Figure S1), **9** (Figure 3), **10** (Figure S18), **11** (Figure 2), and **13** (Figure S26), again exclusively using the O_{amide} instead of the NH_{2amide} function. Thus, in the Pya-containing compounds **9** and **11** both κ^2-*N,O* chelate binding and μ-*O,N* ditopic bridging was observed, while for Pia in compound **8**, the κ^2-*N,O* chelate binding prevented further μ-*O,N* ditopic bridging (Figure 4, middle). For compounds containing Ina or

4-Aba no chelate binding is possible and μ-*O*,*N* ditopic bridging was observed in some cases but not all. Out of the four compounds containing an 1,4-pyrazine unit three of them, **9**, **11**, and **12** show μ-*N*,*N*_{pyrazine}-bridging, while in **10** one pyrazine *N* position does not coordinate. In **12** the same pyrazine-2-carboxylate (Pyc⁻) ligand bridges two Cu^{II} centres in a μ-*N*,*N* fashion, bridges to another Cu^{II} using the carboxylate *O* function (μ-*O*,*O*), and shows κ²-*N*,*O* chelate binding at the same time, while the Tfa⁻ ligand binds terminally (Figure S23).
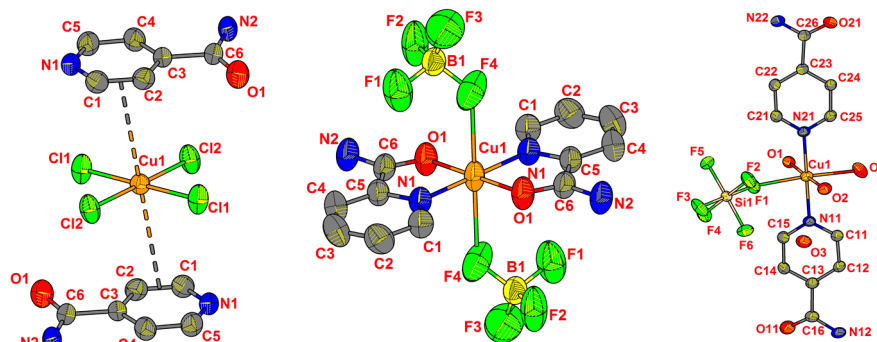

Figure 4. ORTEP representation (50% probability level) of the molecular entities within the structures of (HIna)₂[CuCl₄] 2H₂O (**6**) (**left**) of [Cu(Pia)₂(BF₄)₂] (**8**) (**middle**) and [Cu(Ina)₂(H₂O)₃(SiF₆)]·H₂O (**4**) (**right**); H atoms were omitted for clarity.

Nitrate (NO₃⁻) ligands are frequently found in terminal binding (**2** (Figure 1), **3**, **10**, **11**, **13**). However, in compound **11** one of the two NO₃⁻ ligands binds in a quasi-κ²-*O*,*O* fashion (Figure 2). In **14** both κ²-*O*,*O* and terminal binding were observed.

The thio-bisacetamide (Tba) ligand exhibits tridentate *N^S^N* binding in compound **18** as expected (Figure S39). In (HIna)[Cu(H₂O)Cl₃] (**7**) (Figure S13) the pyridine-*N* protonated HIna⁺ does not coordinate to Cu^{II}. A unique coordination mode is found in (HIna)₂[CuCl₄] (**6**) (Figure 4 and Figure S11) with two HIna⁺ cations occupying the axial positions with the C1=C2 bond of the pyridine ring (Figure 4, left). Although the Cu···C=C_{centroid} distance is rather long (3.360(1) Å) we consider this as a bonding contribution.

In the compounds **1**, **3**, **4**, and **7** containing the Ina ligand and **11** which contains the 4-NH₃ protonated 4-HAba⁺ ligand isolated Cu^{II} complexes were found. In their structures weak intermolecular forces as hydrogen bridges and π–π stacking are observed. Importantly, such forces were found in all compounds and we cannot neglect their role on the geometry around Cu^{II} which is decisive for the physical properties. Nevertheless, these non-covalent forces will not be further discussed, as we wanted to focus on the spectral consequences of the geometry around the Cu centre and not its origin.

The predominant coordination unit around Cu^{II} in most of the compounds reported herein is of the frequently observed tetragonally distorted octahedral type (OE in Table 2) [33,37,41–48]. The short equatorial positions are dominated through the *N* pyridine, pyrazine and aminophenyl functions. *O*_{amide} occurs in this plane only in chelates with these *N* functions, NH₂_{amide}–Cu binding was not observed. The Cu^{II}–ligand bonds in the equatorial plane lie in the range of 1.93 to 2.08 Å and are comparable with previously reported complexes of these ligands [13–32,38–46]. Remarkably, the shortest Cu–ligand bonds were of the Cu–*O*_{amide} type and were found for the chelating Pia, Pya, and 2-Aba ligands, but also for terminating binding of the 4-Aba ligands including the 4-HAba⁺ cation. The Ina ligand forms exclusively short Cu–N bonds, while the *O*_{amide} function does not contribute to the equatorial Cu–ligand bonding. For the compounds containing chlorido ligands, all four equatorial positions were Cl-occupied in (HIna)₂[CuCl₄] (**6**) but at the same time the *O*_{amide} function coordinates tighter than one of the two chlorido ligands in [Cu(4-Haba)₂Cl₄] (**17**). The Cu–Cl distances range from 2.26 to 2.30 Å underlining that Cl⁻ is a reasonably strong ligand to Cu^{II}.

Table 2. Selected binding parameters (distances in Å, angles in °) around the Cu^{II} centres.

Complex	Geometry [a]	T (K)	Cu–L^1 [b]	Cu–L^2	Cu–L^3	Cu–L^4	Cu–L^5	Cu–L^6	
			L^1–Cu–L^2	L^2–Cu–L^3	L^3–Cu–L^4	L^1–Cu–L^5	L^1–Cu–L^6	L^1–Cu–L^3	L^5–Cu–L^6
[Cu(Ina)$_4$(H$_2$O)$_2$](BF$_4$)$_2$ (**1**)	OE	298(2)	2.024(3) N21	2.045(4) N11	=N11	=N21	2.392(5) O1	2.645(5) O2	
			91.7(1)°	88.9(2)°	91.7(1)°	86.5(1)°	93.4(1)°	173.0(1)°	180°
$^1_\infty$[Cu(Ina)$_2$(NO$_3$)$_2$] (**2**)	SPy+1	298(2)	1.987(5) O31	1.994(5) N21	2.002(5) N11	2.004(4) O41	2.314(4) O11	-	
			90.1(2)°	87.7(2)°	89.1(2)°	78.9(2)°	-	165.5(2)°	-
[Cu(Ina)$_2$(H$_2$O)$_2$(NO$_3$)$_2$] (**3**) [c]	OE	296(2)	1.984(1) O2	1.992(1) N1			2.507(1) O3		
			90.0(1)°	90.0(1)°		95.6(1)°	84.4(1)°	180°	180°
[Cu(Ina)$_2$(H$_2$O)$_3$(SiF$_6$)]·H$_2$O (**4**)	OE	298(2)	1.969(2) O1	1.986(2) O2	1.999(2) N21	2.026(2) N11	2.409(2) F1	2.513(2) O4	
			90.1(1)°	89.6(1)°	88.2(1)°	88.2(1)°	84.9(1)°	180°	170.9(1)°
(HIna)$_2$[CuCl$_4$]·2H$_2$O (**6**)	SP+2	298(2)	2.263(1) Cl1	2.270(1) Cl2	=Cl1	=Cl2	3.360(1) = (py)	=L^5	
(HIna)[Cu(H$_2$O)Cl$_3$] (**7**) [c]	SPy	298(2)	1.980(4) O1	2.251(1) Cl2	2.268(1) Cl1	2.279(1) Cl3	2.923(1) Cl2′	-	
			87.4(1)°	93.2(1)°	92.6(1)°	-	-	172.5(1)°	-
[Cu(Pia)$_2$(BF$_4$)$_2$] (**8**)	OE	150(2)	1.935(3) O1	1.958(4) N1	=O1	=N1	2.589(3) F4	=F4	
			83.3(2)°	96.6(1)°	83 (2)°	89.7(1)°	90.3(1)°	180°	180°
$^2_\infty$[Cu(Pya)$_2$(BF$_4$)$_2$] (**9**)	OE	298(2)	1.957(2) O11	1.984(3) N12	=O11	=N12	2.447(3) N11	=N11	
			82.2(1)°	97.7(1)°	82.2(1)°	85.5(1)°	94.4(1)°	180°	180°
[Cu(Pya)$_2$(H$_2$O)(NO$_3$)](NO$_3$) (**10**)	Spy+1	298(2)	1.935(4) O11	1.938(4) O21	1.984(4) N21	1.989(4) N11	2.234(4) O5	2.818(4) O43	
			82.7(1)°	97.6(1)°	82.7(1)°	94.3(2)°	89.7(1)°	172.1(1)°	169.8(1)°
$^1_\infty$[Cu(Pya)(NO$_3$)$_2$] (**11**)	SPy	298(2)	1.953(2) O11	1.979(2) O31	1.998(2) N12	2.004(2) N11	2.238(2) O21	2.572(3) O33	
			81.6(1)°	89.3(1)°	92.3(1)°	91.0(1)°	93.6(1)°	169.2(1)°	136.9(1)°
$^2_\infty$[Cu(Pyc)(Tfa)] (**12**) [d]	SPy	298(2)	1.942(5) O1	1.944(7) O11	1.997(6) O12	2.065(8) N11	2.272(8) N12	-	
			88.8(2)°	97.6(2)°	92.7(3)°	96.5(3)°	-	171.3(2)°	-
[Cu(2-Aba)$_2$(NO$_3$)$_2$] (**13**)	OE	298(2)	1.976(3) O1	2.010(4) N1	=O1	=N1	2.506(5) O3	=O3	
			87.3(2)°	92.7(2)°	87.3(2)°	92.8(1)°	87.1(1)°	180°	180°
$^1_\infty$[Cu$_2$(4-Aba)$_2$(H$_2$O)$_3$(NO$_3$)$_3$](NO$_3$) (**14**) [e]	OD	298(2)	1.942(4) O11	1.969(4) O21	2.016(4) N11	2.034(5) O21	2.262(4) O32	2.35(1) O23	
			89.1(2)°	88.2(2)°	93.3(2)°	82.9(2)°	95.2(3)°	176.0(2)°	143.1(3)°
$^2_\infty$[Cu(4-Aba)$_2$(EtOH)$_2$](ClO$_4$)$_2$ (**15**)	OE	150(2)	1.951(2) O11	2.077(4) N11	=N11	=O11	2.529(2) O21	=O21	
			87.8(1)°	92.1(1)°	87.8(1)°	94.4(1)°	85.5(1)°	180°	180°
$^2_\infty$[Cu(4-Aba)$_2$(EtOH)$_2$](BF$_4$)$_2$ (**16**)	OE	298(2)	1.951(2) O11	2.062(3) N11	=O11	=N11	2.545(2) O1	=O1	
			87.9(1)°	92.1(1)°	87.9(1)°	87.3(1)°	92.6(1)°	180°	180°
[Cu(4-HAba)$_2$Cl$_4$] (**17**) [f]	OE	298(2)	1.957(6) O1	2.313(3) Cl1	=O1	=Cl	2.867(2) Cl2	=Cl2	
			89.6(2)°	90.4(2)°	89.6(2)°	98.2(1)°	81.8(2)°	180°	180°
[Cu(Tba)$_2$](ClO$_4$)$_2$ (**18**)	OE	298(2)	1.976(2) O11	=O11	=O11	=O11	2.625(1) S11	=S11	
			90.9(1)°	89.1(1)°	90.9(1)°	81.5(1)°	98.4(1)°	180°	180°

[a] OE = tetrahedrally elongated octahedral, OD = otherwise distorted octahedral, SPy = square pyramidal, [b] L$_1$ is defined by the shortest Cu–ligand bond, L$_2$ to L$_4$ lie in the equatorial plane, L$_5$ and L$_6$ in the elongated axial positions. [c] Data from [16]. [d] Pyc$^-$ = pyrazine-2-carboxylate. [e] Two species with slightly different bonding parameters. [f] 4-AbaH$^+$ = 4-benzamidyl ammonium.

For the labelling of the structures as OE in Table 2, two axial ligands must be present in a distance elongated to about 10–20% compared to the same ligand in an equatorial position [42]. Further observed cases were square pyramidal structures (Spy in Table 2), two structures containing one long axial and one even longer axial Cu–ligand bond (Spy+1) and the peculiar case of two very long distances to Cu^{II} as in (HIna)$_2$[CuCl$_4$] (**6**) (Figure 4, left) called square planar +2 (SQ+2). In compound **10** (Figure S19)

the sixth ligand is not only elongated but also displaced from the ideal position showing an "axial" angle of about 170°. Nevertheless, we assign this to Spy+1. In **14** (Figure S30) the coordination around Cu^{II} showed a severely and multiply distorted octahedron (OD).

Non-chelated O_{amide} binding to Cu^{II} was found in the axial (weak) positions only in one compound (**2**) and no NH_{2amide} coordination, in line with the observation that amide functions in amino acids do not represent an important class of ligands in metalloproteins [34–36] and the poor non-biologic coordination chemistry of amides and Cu [33,35,37]. Indeed, searching the CCDC database, gave only the Cu^{II} complex [Cu(L)$_2$(OH)$_2$] containing two chelating pyrazine-2,3-dicarboxamide ligands with Cu–NH_{2amide} bonds [49]. Further frequent ligands in the axial positions of our structures were weak ligands as NO$_3^-$, EtOH, H$_2$O, BF$_4^-$, and the peculiar SiF$_6^{2-}$ (Figure 4). Nevertheless, the non-chelating $N_{4pyrazine}$ function of the Pyc$^-$ ligand (in **12**) was found in the axial position. Importantly, the axial non-chelating O_{amide} (in **2**) and $N_{4pyrazine}$ binding (in **12**) both represent structures with μ-O,N ditopic bridging. The axial position is occupied by the thio-bisacetamide (Tba) S atoms in compound **18** in line with the preferences of Cu^{II} to N over S coordination [33,34,50].

2.3. X-Band EPR Spectroscopy and Magnetic Measurements

X-Band EPR spectra of the microcrystalline materials were recorded at 298 and 110 K, Figures 5 and 6 show representative examples, Table 3 lists essential parameters.
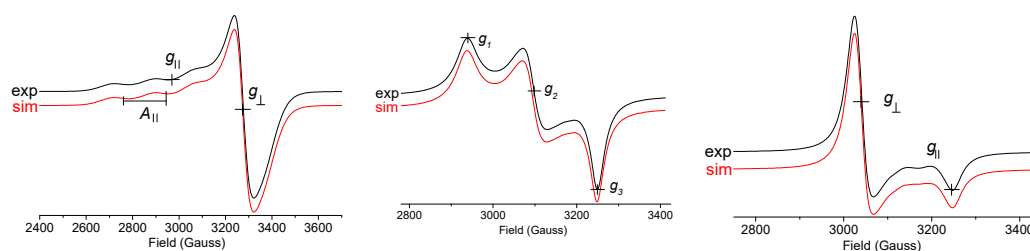

Figure 5. X-band EPR spectra of microcrystalline samples of [Cu(Ina)$_4$(H$_2$O)$_2$](BF$_4$)$_2$ (**1**) (**left**, frequency = 9.455063 GHz, simulation in red with parameters in Table 3), (Cu(H-Aba)$_2$Cl$_4$) (**17**) (**middle**, frequency = 9.454244 GHz, simulation in red), and [Cu$_2$(Aba)$_2$(H$_2$O)$_3$(NO$_3$)$_3$](NO$_3$) (**14**) (**right**, frequency = 9.448669 GHz, simulation in red), all measured at 298 K.
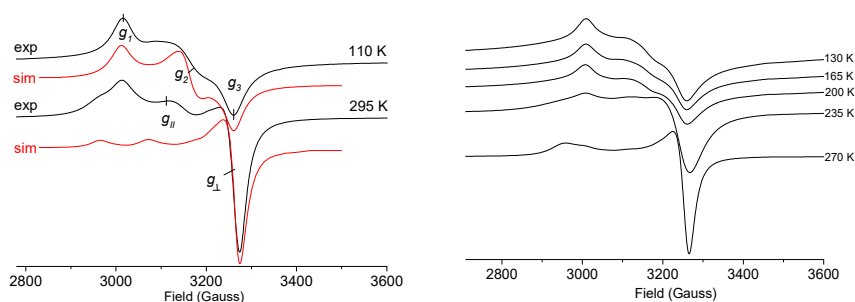

Figure 6. X-band EPR spectra of a microcrystalline sample of [Cu(4-Aba)$_2$(EtOH)$_2$](ClO$_4$)$_2$ (**15**) at 110 K (frequency = 9.459916 GHz) and 295 K (frequency = 9.448669 GHz) both with simulations in red (**left**) and at temperatures ranging from 130 to 270 K (**right**).

Table 3. Selected X-band EPR data of Cu^{II} compounds.[a]

Compound	T (K)	g_{av}	$g_∥/g_1$	g_2	$g_⊥/g_3$	Δg	Spectral Geom.	Cu^{II} Geom.
Group I								
[Cu(Ina)$_2$(NO$_3$)$_2$] (**2**)	298	2.143	2.280		2.074	0.206	axial	SPy+1
[Cu(Ina)$_4$(H$_2$O)$_2$](BF$_4$)$_2$ (**1**) [b]	298	2.118	2.260		2.048	0.212	axial	OE
(HIna)$_2$[CuCl$_4$]·2H$_2$O (**6**)	298	2.132	2.266	2.082	2.047	0.219	rhombic	SP+2
[Cu(Ina)$_2$(H$_2$O)$_3$(SiF$_6$)]·H$_2$O (**4**)	298	2.154	2.326		2.068	0.258	axial	OE
[Cu(Ina)$_2$(H$_2$O)$_2$(NO$_3$)$_2$] (**3**)	298	2.156	2.297		2.085	0.212	axial	OE
[Cu(4-HAba)$_2$Cl$_4$] (**17**)	298	2.175	2.286	2.169	2.066	0.219	rhombic	OE
[Cu(Pya)(NO$_3$)$_2$] (**11**)	298	2.179	2.372		2.083	0.289	axial	SPy
[Cu(Pya)$_2$(H$_2$O)(NO$_3$)](NO$_3$) (**10**)	298	2.183	2.400		2.075	0.325	axial	SPy+1
similar compounds								
[Cu(CCl$_3$COO)$_2$(MNA)$_2$]·2H$_2$O [c]	298	2.143	2.280		2.075	0.205	axial	OE
[Cu(Ina)$_2$(μ-N,S-SCN)$_2$] [d]	298	2.20	2.27		2.07	0.200	axial	OE
[Cu(meclof)$_2$(2-pyca)$_2$] [e]	298	2.142	2.290		2.068	0.222	axial	OE
[Cu(clof)$_2$(4-pymeth)$_2$(H$_2$O)] 2H$_2$O [f]	298	2.128	2.271		2.054	0.217	axial	SPy
[Cu(clof)$_2$(Et$_2$nia)$_2$] [f]	298	2.132	2.289		2.053	0.236	axial	[g]
[Cu(clof)$_2$(Ina)$_2$] [f]	298	2.153	2.285		2.087	0.198	axial	[g]
[Cu(tolf)$_2$(Et$_2$nia)$_2$)(H$_2$O)$_2$] [h]	298	2.130	2.294		2.048	0.246	axial	OE
[Cu(tolf)$_2$(Nia)$_2$] [h]	298	2.157	2.319		2.076	0.243	axial	[g]
Group II								
[Cu(Pya)$_2$](BF$_4$)$_2$ (**9**)	298	2.140	2.204	2.139	2.078	0.126	rhombic	OE
[Cu(4-Aba)$_2$(EtOH)$_2$](ClO$_4$)$_2$ (**15**)	110	2.137	2.231	2.123	2.059	0.172	rhombic	OE
[Cu(4-Aba)$_2$(EtOH)$_2$](ClO$_4$)$_2$ (**15**)	298	2.111	2.200		2.066	0.133	axial	OE
[Cu(4-Aba)$_2$(EtOH)$_2$](BF$_4$)$_2$ (**16**)	110	2.139	2.220	2.140	2.058	0.162	rhombic	OE
[Cu(4-Aba)$_2$(EtOH)$_2$](BF$_4$)$_2$ (**16**)	298	2.110	2.196		2.068	0.131	axial	OE
[Cu(TBA)$_2$](ClO$_4$)$_2$ (**18**)	298	2.130	2.228		2.080	0.147	axial	OE
similar compounds								
[Cu$_2$(Ina)$_2$(μ-1,1-N$_3$)$_2$(μ-1,3-N$_3$)$_2$] [d]	298	2.17	2.22		2.07	0.150	axial	SPy+1
[Cu(Ina)$_2$(μ-1,1-N$_3$)$_2$(μ-O,O-SO$_4$)]·2H$_2$O [d]	298	2.17	2.24	2.18	2.09	0.150	rhombic	SPy
Group III								
[Cu(Pyc)(Tfa)] (**12**)	298	2.138		2.138		0	isotropic	SPy
[Cu(Ina)$_2$Br$_2$] (**5**)	298	2.111		2.111		0	isotropic	SPy [i]
Group IV								
[Cu$_2$(Aba)$_2$(H$_2$O)$_3$(NO$_3$)$_3$](NO$_3$) (**14**)	298	2.141	2.190		2.050	0.112	inv. axial	OD

[a] Measured at 298 K or 110 K on microcrystalline powders; g_{av}= averaged g value = ($g_∥$+ $2g_⊥$)/3 or (g_1 + g_2 + g_3)/3; Δg = $g_∥$− $g_⊥$ or g_1 − g_3. OE = tetragonal elongated octahedral, OD = otherwise distorted octahedral, SPy = square pyramidal. [b] An HFS $A_∥$ of 180 G was observed. [c] From [20]; MNA = *N*-methylnicotinamide; an HFS $A_∥$ of 165 G is observed. [d] From [15]. [e] From [18]; meclof = meclofenamate; 2-pyca = 2-pyridylcarbinol. [f] From [24]; clof = 2-(4-chlorophenoxy)-2-methylpropionic acid; 4-pymeth = 4-pyridylmethanol, Et$_2$nia = *N,N*-diethylnicotinamide, an HFS $A_∥$ of 165 G is observed for [Cu(clof)$_2$(Et$_2$nia)$_2$]. [g] No structure reported. [h] From [17], tolf = tolfenamic (*N*-(2-methyl-3-chlorophenyl)anthranilic) acid. [i] No unequivocal structure from XRD (see text); previous assignment OE from powder XRD and IR, [22].

EPR spectra of axial, rhombic and isotropic geometry were observed and, having full structural information from XRD, will be correlated to the local environment of the Cu^{II} centres in the following.

EPR spectra of axial symmetry with $g_∥ > g_⊥$ (Group I in Table 3, Figure 5 (left)) were observed for most of the tetragonally elongated octahedral species (OE) and square pyramidal systems with an extra-long distance to a sixth ligand (SPy+1) in line with previous reports [24,41–52]. Cu hyper

fine structure (HFS, coupling to the ^{63}Cu (69.17%) and ^{65}Cu (30.83%) nuclei both with $I = 3/2$ [53]) was only observed in one case, $[Cu(Ina)_4(H_2O)_2](BF_4)_2$ (Figure 5 (left)), on the parallel g component ($A_{\parallel} = 180$ G). The prevailing absence of HFS is in line with spectra of related species in the solid (see Table 3) [15–18,20,24]. The g anisotropy (Δg) in this group of complexes lies above values of 0.2 while the averaged g values (g_{av}) vary from 2.12 to 2.20. Exceptions are $(HIna)_2[CuCl_4]\cdot 2H_2O$ (**6**) and $[Cu(H–Aba)_2Cl_4]$ (**17**) for which a rhombic spectrum was observed (Figure 5 (middle) and Figure S43). On the other hand, the Δg values lie in the same range as for compounds of group I.

Rhombic spectra were recorded for $[Cu(Pya)_2](BF_4)_2$ (**9**), $[Cu(4-Aba)_2(EtOH)_2](ClO_4)_2$ (**15**) and $[Cu(4-Aba)_2(EtOH)_2](BF_4)_2$ (**16**) (group IV) when measured at 110 K (group II). Remarkably, the spectra of the two latter compounds are axial at 298 K and for $[Cu(4-Aba)_2(EtOH)_2](ClO_4)_2$ (**15**) a gradual transition between the rhombic and axial spectrum was observed between 110 and 298 K (Figure 6). The Δg values for this group of complexes lie markedly below 0.2 and their g_{av} values range from 2.1 to 2.17. A detailed inspection of the metrics around Cu^{II} showed very similar geometries for $[Cu(4-Aba)_2(EtOH)_2](ClO_4)_2$ (**15**) at 150 K and $[Cu(4-Aba)_2(EtOH)_2](BF_4)_2$ (**16**) at 298 K. We therefore concluded that in this group either very tiny changes in geometry and with this a change of the character of the electronic ground state from the predominant $\{dx^2\text{-}y^2\}^1$ (axial) to a $\{dz^2\}^1$ electronic ground state (rhombic or inverse axial) [42,47,48,54,55] were decisive and axial or rhombic spectra were observed. Importantly, this group is defined by a rather low g anisotropy Δg.

An isotropic broad spectrum with g values around 2.15 was observed for $[Cu(Pyc)(Tfa)]$(**12**) containing a square pyramidally coordinated Cu^{II} (group III). An isotropic spectrum was also found for the structurally ill-defined $[Cu(Ina)_2Br_2]$ (**5**). Our findings for **5** are in line with the reported spectrum and g values for this compound by Atac et al. [22], while for the $[Cu(Ina)_2Cl_2]$ derivative this group reports a rhombic spectrum. From our EPR results we conclude a square pyramidal coordination for Cu^{II} in $[Cu(Ina)_2Br_2]$ (**5**).

A rather uncommon inverse axial EPR spectrum was observed for $[Cu_2(Aba)_2(H_2O)_3(NO_3)_3](NO_3)$ (**14**). This type of symmetry is frequently observed for either axially compressed octahedral structures, $\{dz^2\}^1$ ground states, or both, in contrast to the predominant $\{dx^2\text{-}y^2\}^1$ and axially elongated octahedral coordination [38,48,54,55]. However, this structure represents several marked distortions from octahedral geometry, but not a compression. So, we can conclude a $\{dz^2\}^1$ electronic ground state for the two Cu^{II} centres in this compound.

We selected the samples $[Cu(Ina)_2(NO_3)_2]$ (**2**), $[Cu(Pya)(NO_3)_2]$ (**11**), $[Cu(Pyc)(Tfa)]$(**12**), and $[Cu(4-Aba)_2(EtOH)_2](ClO_4)_2$ (**15**) for T-dependent magnetic measurements (Figure 7). **2** and **11** are 1D structures, while **12** and **15** represent 2D coordination polymers. Above 150 K a linear Curie-Weiss dependence is observed, in line with isolated Cu^{II} centres. At lower T, slight deviations were observed and the χ^{-1} graph tails down to zero, indicative for small anti-ferromagnetic coupling between the Cu centres in the solids. The shortest Cu$\cdots$Cu contacts are 7.083 (1) Å (**2**), 5.822 (1) Å (**11**), 5.118 (2) and 7.079 (2) Å (**12**), and 8.463 (3) Å (**15**) and thus far too long for a super-exchange magnetic coupling. We assume that the alignment of the Cu^{II} centres in the 1D and 2D lattices is responsible for this effect. The magnetic moments (Table 4) are markedly below the spin-only value of 1.73 and positive Curie-Weiss constants are in line with this assumption. In contrast to this, for $[Cu(Ina)_2Br_2]$ a μB of 1.90 has been reported alongside with $[Cu(Ina)Cl_2]$ and $[Cu(Ina)(NCS)_2]$ with 1.80 and 1.60 μB, respectively [39]. Higher values were due to spin-orbit coupling which is caused through heavy atoms such as Br or Cl. For our compounds only light N, O, or F atoms bind to Cu^{II} [3,5,10,15,19,52,56].
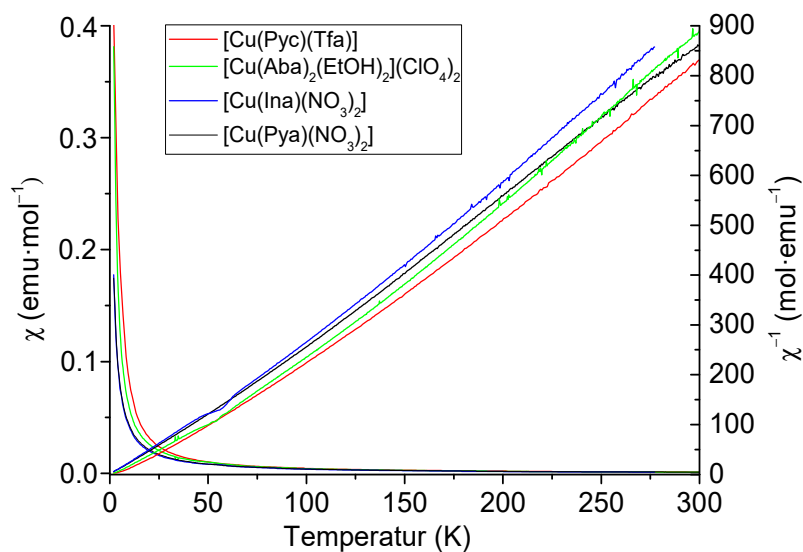
Figure 7. Thermal dependence of χ and χ^{-1} of selected Cu^{II} compounds.

Table 4. Magnetic moments and Curie-Weiss constants of selected Cu^{II} compounds.[a]

Compound	μ_B	θ_{CW} (K)	EPR Symmetry	Symmetry Around Cu^{II}
$[Cu(Ina)_2(NO_3)_2]$ (**2**)	1.50	36.9	axial	SPy + 1
$[Cu(Pya)(NO_3)_2]$ (**11**)	1.65	6.55	isotropic	SPy
$[Cu(Pyc)(Tfa)]$ (**12**)	1.56	48.3	isotropic	SPy
$[Cu(Aba)_2(EtOH)_2](ClO_4)_2$ (**15**)	1.52	42.8	axial	OE

[a] Magnetic moments in Bohr magnetons μB and Curie-Weiss constants θ_{CW} in K.

2.4. Absorption Spectroscopy in the Solid and in Solution

All microcrystalline materials show colours corresponding to absorptions in the visible region. UV-vis absorption spectroscopy on selected samples (Table 5) reveals low-wavelengths absorptions ranging from 640 to 780 nm (15,600 to 12,820 cm^{-1}) which were assigned to the typical Cu^{II} d^9 system. Comparison of the three Pya-containing species reveals that the highest absorption energy is recorded for $[Cu(Pya)_2](BF_4)_2$ (**9**) with a tetrahedrally elongated (OE) structure, followed by $[Cu(Pya)_2(H_2O)(NO_3)](NO_3)$ (**10**) having an SPy+1 configuration with the sixth ligand markedly elongated, while $[Cu(Pya)(NO_3)_2]$ (**11**) exhibits a maximum red-shifted by 2810 cm^{-1} in line with its square pyramidal (SPy) coordination. The long-wavelength absorption observed for $[Cu(Pyc)(Tfa)]$(**12**) is rather high in energy in view of the only five coordinating atoms. This is probably due to the Tfa$^-$ ligand with a very short Cu–O distance indicative for its binding strength. For $[Cu(Ina)_2Br_2]$ we found approximately the same absorption maximum as reported [22] in keeping with the assumption that we have obtained the same structure.

A view of a collection of similar structures (Table 5) confirmed that the absorption energy increased with increasing coordination number for very similar O and N coordinating pyridine-amides. For the unknown structures $[Cu(clof)_2(Et_2nia)_2]$ [18] and $[Cu(meclof)_2(Et_2nia)_2]$ [24], elongated octahedral coordination can be reasonably assumed from the UV-vis data, while the structure of $[Cu(clof)_2(Ina)_2]$ probably represents a square pyramid.

Table 5. UV-vis absorption maxima of selected copper complexes.[a.]

Compound	λ (nm/cm⁻¹) of d-d Bands	Colour of the Crystals	Symmetry Around Cu[II b]
[Cu(Pya)₂](BF₄)₂ **(9)**	613/16,310	blue	OE
[Cu(Pya)₂(H₂O)(NO₃)](NO₃) **(10)**	640/15,630	blue	SPy + 1
[Cu(Pya)(NO₃)₂] **(11)**	780/12,820	blue	SPy
[Cu(Pyc)(Tfa)] **(12)**	664/15,060	turquoise	SPy
[Cu(Ina)₂Br₂] **(5)**	691/14,470	dark green	-[b]
similar compounds			
[Cu(tolf)₂(Et₂nia)₂)(H₂O)₂] [c]	614/16,290	blue	OE
[Cu(meclof)₂(2-pyca)₂] [d]	615/16,260	blue	OE
[Cu(meclof)₂(Et₂nia)₂] [d]	605/16,530	blue	-[e]
[Cu(clof)₂(4-pymeth)₂(H₂O)] 2H₂O [f]	620/16,130	blue	SPy
[Cu(clof)₂(Ina)₂] [f]	660/15,150	blue	-[e]
[Cu(clof)₂(Et₂nia)₂] [f]	603/16,580	violet	-[e]

[a] Measured as KBr pellets. [b] OE = tetrahedrally elongated octahedral, SPy = square pyramidal. [b] No unequivocal structure from XRD (see text); previous assignment OE from powder XRD and IR, [22], reported absorption at 675 nm/14,800 cm⁻¹. [c] From [17], tolf = tolfenamic (*N*-(2-methyl-3-chlorophenyl)anthranilic) acid. [d] From [18]; meclof = meclofenamate; 2-pyca = 2-pyridylcarbinol, Et₂nia = *N,N*-diethylnicotinamide. [e] No structure reported. [f] From [24]; clof = 2-(4-chlorophenoxy)-2-methylpropionic acid; 4-pymeth = 4-pyridylmethanol.

3. Experimental Section

3.1. Methods and Instrumentation

^{1}H and ^{13}C NMR spectra were recorded in DMSO-d_6 using a Bruker Avance II 300 spectrometer (Bruker, Rheinhausen, Germany). Elemental analyses were carried out using a HEKAtech CHNS EuroEA 3000 Analyzer (Hekatech, Wegberg, Germany). IR spectra were recorded using KBr or polyethylene pellets using an IFS/66v/S or an Alpha-T spectrometers (Bruker, Rheinhausen, Germany). UV-vis absorption spectra were measured on transparent KBr pellets using a Shimadzu UV-3600 photo spectrometer (Shimadzu Europe, Duisburg, Germany). EPR spectra were recorded in the X-band on a Bruker System ELEXSYS 500E equipped with a Bruker Variable Temperature Unit ER 4131VT (500 to 100 K) (Bruker, Rheinhausen, Germany). The *g* values were calibrated using a dpph sample. The magnetic measurements were carried out on finely ground samples using a MPMS XL7 (Quantum Design, Darmstadt, Germany) instrument measuring from 2 to 300 K at a magnetic field of 1 T.

3.2. Single Crystal Structure Determination

The measurements were performed at 293(2) K or 110(2) K using graphite monochromatised Mo-Kα radiation (λ = 0.71073 Å) on an IPDS II instrument (STOE & Cie., Darmstadt, Germany). The structures were solved by dual space methods using ShelXT-2015 [57] and refined by full-matrix least-squares techniques against F^2 (SHELXL-2017/1) [58,59]. The numerical absorption corrections (X-RED V1.31; STOE & Cie, 2005, Darmstadt, Germany) were performed after optimising the crystal shapes using the X-SHAPE V1.06 (STOE & Cie, 1999, Darmstadt, Germany) [60,61]. The non-hydrogen atoms were refined with anisotropic displacement parameters. H atoms were included by using appropriate riding models. More details on the crystal structures is provided in the Supplementary Materials. CCDC 1058949–1058951, 1058953–1058957, 1058960–1058963, and 2025467–2025471 contain the full crystallographic data. These data can be obtained free of charge at www.ccdc.cam.ac.uk/conts/retrieving.html or from the Cambridge Crystallographic Data Centre, 12 Union Road, Cambridge, CB2 1EZ UK. Fax: +44-1223-336-033; Email: deposit@ccdc.cam.ac.uk.

3.3. Powder X-ray Diffraction (PXRD)

Data collection was carried out with a Huber G670 diffractometer (Huber, Rimsting, Germany) equipped with a Ge(111) monochromator using Cu-Kα1 radiation with λ = 1.5405 Å and an image

plate detector. The samples were measured as flat samples between two almost X-ray transparent foils. The foil gives rise to two broad reflections at $2\theta \approx 21.5°$ and $2\theta \approx 23.7°$. PXRD data were visualised with the WinXPOW software package (STOE & Cie., 2012, Darmstadt, Germany) [62], which was also used to calculate line diagrams based on single crystal data. Gnuplot4.6 was used for the visualisation of PXRD patterns [63].

3.4. Syntheses

3.4.1. General

Picolinamide and nicotinamide were synthesised from their (commercially available) carboxylic acids (details in the Supplementary Materials), all other chemicals were used as supplied. Water-free reactions were carried out under inert gas conditions and performed using Schlenk techniques. Solvents were dried using an MBRAUN MB SPS-800 (MBRAUN, Garching, Germany) solvent purification system.

3.4.2. Synthesis of the Cu^{II} Compounds—General Method

The following compounds were synthesised through dissolving suitable Cu^{II} salts in EtOH, heating these solutions to 70 °C and then slowly adding the ligands to the mixture. Upon standing and slow evaporation of the solvent at ambient temperatures in the fume hood, the materials were obtained in yields from 39 to 75% referring to the Cu^{II} starting material and from 30 to 90% referring to the ligand.

$[Cu(Ina)_4(H_2O)_2](BF_4)_2$ (**1**). From 0.690 g (2 mmol) $Cu(BF_4)_2 \cdot 6H_2O$ and 0.122 g (1 mmol) Ina. Yield: 0.624 g (0.82 mmol, 41% referred to Cu and 82% to Ina) blue plates. Elemental analysis calculated for $C_{24}H_{28}B_2Cu_1F_8N_8O_6$ (761.69): C 37.85, H 3.71, N 14.71; found: C 37.83, H 3.70, N 14.71%. IR (KBr pellet): 3421 s; 3292 m, $\nu_{as}(NH_2)$; 3196 s, $\nu_s(NH_2)$; 3072 sh, $\nu(pyr–H)$; 1678 s, $\nu(C=O)$; 1606 s, $\delta(NH_2)$; 1554 s, 1549 s, $\nu(C=C)$, $\nu(C=N)$; 1425 sh, $\nu(C–C)$; 1415 s, $\nu(C–N)$; 1080 s, $\nu(B–F)$; 639 s, $\delta(N–C=O)$ cm^{-1}. PXRD is available in the Supplementary Materials.

$[Cu(Ina)_2(NO_3)_2]$ (**2**). From 0.481 g (2 mmol) $Cu(NO_3)_2 \cdot 3H_2O$ and 0.122 g (1 mmol) Ina. Yield: 0.337 g (0.78 mmol, 39% referred to Cu and 78% to Ina), blue plates. Elemental analysis calculated for $C_{12}H_{12}Cu_1N_6O_8$ (431.81): C 33.38, H 2.80, N 19.46; found: C 33.36, H 2.81, N 19.44%. IR (PE pellet): 3426 s, 3311 m, $\nu_{as}(NH_2)$; 3181 s, $\nu_s(NH_2)$; 3082 m, $\nu(pyr–H)$; 1705 s, $\nu(C=O)$; 1623 s, $\delta(NH_2)$; 1614 s, 1546 s, $\nu(C=C)$, $\nu(C=N)$; 1424 s, $\nu(C–C)$; 1381 s, $\nu(C–N)$; 1383 s, $\nu(NO_3^-)$; 1118 m, $\nu(CN)$; 484 s, $\delta(N–C=O)$ cm^{-1}.

$[Cu(Ina)_2(H_2O)_2(NO_3)_2]$ (**3**). From 0.482 g (2 mmol) $Cu(NO_3)_2 \cdot 3H_2O$ and 0.144 g (1 mmol) Ina. Yield: 0.383 g (0.82 mmol, 41% referred to Cu and 82% to Ina), blue blocks. Elemental analysis calculated for $C_{12}H_{16}Cu_1N_6O_{10}$ (467.84): C 30.81, H 3.45, N 17.96; found: C 30.83, H 3.46, N 17.94%. The compound was previously reported and obtained from a 1:2 mixture of Cu:ligand [16].

$[Cu(Pia)_2(BF_4)_2]$ (**8**). From 0.690 g (2 mmol) $Cu(BF_4)_2 \cdot 6H_2O$ and 0.122 g (1 mmol) Pia. Yield: 0.385 g (0.8 mmol, 40% referred to Cu and 80% to Pia) light blue plates. Elemental analysis calculated for $C_{12}H_{12}B_2Cu_1F_8N_4O_2$ (481.41): C 29.94, H 2.51, N 11.64; found: C 29.89, H 2.50, N 11.63%. IR (KBr pellet): 3415 m, 3247 m, 3024 m, $\nu(NH_2)$; 1666 s, $\nu(C=O)$; 1560 s, 1444 s, $\nu(C=C)$, $\nu(C=N)$; 1311 w, $\nu(C=N)$; 1072 s, $\nu(B–F)$; 906 sh, $\nu(C–N)$ ring; 767 m, $\delta(C–N)$ ring; 656 m, $\delta(N–C=O)$ cm^{-1}. PXRD is available in the Supplementary Materials.

$[Cu(Pya)_2](BF_4)_2$ (**9**). From 0.345 g (1 mmol) $Cu(BF_4)_2 \cdot 6H_2O$ and 0.123 g (1 mmol) Pya. Yield: 0.208 g (0.43 mmol, 43% referred to Cu and 86% to Pya) light blue plates. Elemental analysis calculated for $C_{10}H_{10}B_2Cu_1F_8N_6O_2$ (483.38): C 24.85, H 2.09, N 17.39; found: C 24.88, H 2.10, N 17.36%. IR (KBr pellet): 3400 m, 3276 s, $\nu_{as}(N–H)$; 3239 s, $\nu_s(N–H)$; 1697 s, $\nu(C=O)$; 1619 m, $\nu(NH_2)$; 1578 m, 1542 w, 1496 m, $\nu(C=C)$, $\nu(N=C)$; 1414 m; 1459 m, amide; 1212 w, $\delta(CH)$; 1182 m, $\nu_{14}(ring)$; 1108-985 vs, $\nu(B–F)$; 871 m, $\gamma(CH)$; 780 m, $\delta(OH)+\nu_1(ring)$; 666 w, $\omega(NH_2)$; 602 m, $\delta(N–C=O)$; 456 m, $\nu_{16}(ring)$ cm^{-1}; $\delta(NH_2)$ and $\delta(CH)$ were probably obscured. PXRD is available in the Supplementary Materials.

[Cu(Pya)$_2$(H$_2$O)(NO$_3$)](NO$_3$) (**10**). From 0.482 g (2 mmol) Cu(NO$_3$)$_2$·3H$_2$O and 0.123 g (1 mmol) Pya. Yield: 0.406 g (0.9 mmol, 45% referred to Cu and 90% to Pya) blue plates. Elemental analysis calculated for C$_{10}$H$_{12}$Cu$_1$N$_8$O$_9$ (451.80): C 26.58, H 2.68, N 24.80; found: C 26.51, H 2.66, N 24.75%. IR (KBr pellet): 3600–2975 m, ν(O–H) H$_2$O; 3339 m, ν_{as}(N–H); 3150 s, ν_s(N–H); 1681 s, ν(C=O); 1605 s, ν(NH$_2$); 1567 m, 1530 w, 1492 m, ν(C=C), ν(N=C); 1449 s, 1397 m, amide; 1350 s, ν(NO$_3^-$); 1199 w, δ(CH); 1175 m, ν_{14}(ring); 1081 m, δ(NH$_2$); 1058 s, δ(CH); 1022 sh, ν_{12}(ring); 882 m, γ(CH); 803 m, δ(OH)+ν_1(ring); 690 w, ω(NH$_2$); 641–561 m, δ(N–C=O); 467 m, ν_{16}(ring) cm^{-1}. PXRD is available in the Supplementary Materials.

[Cu(Pya)(NO$_3$)$_2$] (**11**). From 0.241 g (1 mmol) Cu(NO$_3$)$_2$·3H$_2$O and 0.123 g (1 mmol) Pya. Yield: 0.233 g (0.245 mmol, 75% referred to Cu and Pya) blue plates. Elemental analysis calculated for C$_5$H$_5$Cu$_1$N$_5$O$_7$ (310.67): C 19.33, H 1.62, N 22.54; found: C 19.31, H 1.64, N 22.51%. IR (KBr pellet): 3386 m, 3287 s, ν_{as}(N–H); 3090 s, ν_s(N–H); 1693 s, ν(C=O); 1630 m, ν(NH$_2$); 1599 m, 1543 w, ν(C=C), ν(N=C); 1310 s, amide; 1212 w, δ(CH); 1488 s, 1421 s, 1282 s, ν(NO$_3^-$); 1116 m, ν_{14} ring; 1077 m, δ(NH$_2$); 1058 s, δ(CH); 1021 s, ν_{12} ring; 871 m, γ(CH); 803 m, δ(OH)+$\nu1$(ring); 689 m, ω(NH$_2$); 483 w, δ(N–C=O) cm^{-1}.

[Cu(Pyc)(Tfa)](**12**). From 0.308 g (1 mmol) Cu(Tfa)$_2$·H$_2$O and 0.123 g (1 mmol) Pya. Yield: 0.263 g (0.88 mmol, 88% referred to Cu and Pya) blue blocks. Elemental analysis calculated for C$_7$H$_3$Cu$_1$F$_3$N$_2$O$_4$ (299.65): C 28.06, H 1.01, N 9.35; found: C 28.08, H 1.04, N 9.33%. IR (KBr pellet): 3236 s, ν(ring–H); 1696 vs, ν(C=O) of Tfa; 1728 s ν(C=O) of Pyc; 1587 m, 1520 m, 1440 m, ν(C=C), ν(N=C); 1207–1138 s, ν(C–F); 1065 w, δ(CH); 1047 m, ν_{12}(ring); 867 sh; γ(CH); 779 sh, δ(OH)+ν_1(ring); 468 m, ν_{16}(ring) cm^{-1}; Not observed (obscured): ν_{as}(N–H), ν_s(N–H), ν(NH$_2$), amide, δ(CH), δ(NH$_2$), ω(NH$_2$), and δ(N–C=O). FIR (KBr pellet): 614 m, ring; 580 m, ν_1(Cu–O); 516 m, ν_2(Cu–O); 475 m, ring; 420 m, ν_3(Cu–O); 317 m, ν_1(Cu–N11); 291 s, ν_2(Cu–N12) cm^{-1}. PXRD is available in the Supplementary Materials.

[Cu(2-Aba)$_2$(NO$_3$)$_2$] (**13**). From 0.241 g (1 mmol) Cu(NO$_3$)$_2$·3H$_2$O and 0.136 g (1 mmol) 2-Aba. Yield: 0.202 g (0.44 mmol, 44% referred to Cu and 88% to 2-Aba) green plates. Elemental analysis calculated for C$_{14}$H$_{16}$Cu$_1$N$_6$O$_8$ (459.86): C 36.57, H 3.51, N 18.28; found: C 36.55, H 3.54, N 18.30%. PXRD is available in the Supplementary Materials.

(Cu$_2$(4-Aba)$_2$(NO$_3$)$_3$(H$_2$O)$_3$)(NO$_3$) (**14**). From 0.241 g (1 mmol) Cu(NO$_3$)$_2$·3H$_2$O and 0.136 g (1 mmol) 4-Aba, Yield: 0.295 g (0.42 mmol, 84% referred to Cu and 4-Aba) green needles. Elemental analysis calculated for C$_{14}$H$_{22}$Cu$_2$N$_6$O$_8$ (701.46): C 23.97, H 3.16, N 15.97; found: C 23.98, H 3.13, N 15.97%.

[Cu(4-Aba)$_2$(EtOH)$_2$](ClO$_4$)$_2$ (**15**). From 0.370 g (1 mmol) Cu(ClO$_4$)$_2$·6H$_2$O and 0.408 g (3 mmol) 4-Aba.Yield: 0.564 g (0.90 mmol, 90% referred to Cu and 30% to 4-Aba) green blocks. Elemental analysis calculated for C$_{18}$H$_{28}$Cl$_2$Cu$_1$N$_4$O$_{12}$ (626.88): C 34.49, H 4.50, N 8.94; found: C 34.48, H 4.52, N 8.93%. IR (KBr pellet): 3441 s, ν(O–H) EtOH; 3362 ms; 3292 s, ν_{as}(N–H); 3252 m, ν_s(N–H); 3058 m, ν(aryl–H); 1650 s, 1611 s, ν(C=O), δ(NH$_2$); 1550 s, ν(C=C) ring; 1450 s, $\delta_{s,as}$(CH$_2$,CH$_3$) EtOH; 1197-992 vs, ν(C–O) EtOH; 1046 s, 620 m, ClO$_4^-$ cm^{-1}; δ(N–C=O) probably obscured. PXRD is available in the Supplementary Materials.

[Cu(4-Aba)$_2$(EtOH)$_2$](BF$_4$)$_2$ (**16**). From 0.345 g (1 mmol) Cu(BF$_4$)$_2$·6H$_2$O and 0.408 g (3 mmol) 4-Aba. Yield: 0.553 g (0.92 mmol, 92% referred to Cu and 31% to 4-Aba) green blocks. Elemental analysis calculated for C$_{18}$H$_{28}$B$_2$Cu$_1$F$_8$N$_4$O$_4$ (601.60): C 35.94, H 4.69, N 9.31; found: C 35.93, H 4.66, N 9.33%. IR (KBr pellet): 3450 s, ν(O–H) EtOH; 3379 m, 3319 s, ν_{as}(N–H); 3277 s, ν_s(N–H); 3175 m, ν(aryl–H); 1652 s, 1610 s, ν(C=O), δ(NH$_2$); 1555 s, ν(C=C) ring; 1453 s, $\delta_{s,as}$(CH$_2$,CH$_3$) EtOH; 1199-911 s, ν(C–O) EtOH, ν(B–F) cm^{-1}. PXRD is available in the Supplementary Materials.

[Cu(4-HAba)$_2$Cl$_4$] (**17**). From 0.370 g (1 mmol) Cu(ClO$_4$)$_2$·6H$_2$O and 0.136 g (1 mmol) 4-Aba and 5 mL concentrated aqueous HCl. Yield: 0.206 g (0.43 mmol, 43% referred to Cu and 86% to 4-Aba) brown platelets. Elemental analysis calculated for C$_{14}$H$_{18}$Cl$_4$Cu$_1$N$_4$O$_2$ (479.67): C 35.06, H 3.78, N 11.68; found: C 35.03, H 3.77, N 11.67%. IR (KBr pellet): 3378 s, ν_{as}(N–H); 3001-2650 s, ν_s(N–H); 2580–2560 m, ν(N–H) amine; 1650 s, 1611 m, ν(C=O), δ(NH$_2$); 1550 m, ν(C=C) ring; 579 m,

δ(N–C=O) cm^{-1}. FIR (KBr pellet): 547 m, ν_1(Cu–O); 473 m, ring; 380 m, ν_2(Cu–O); 318 m, ν_1(Cu–Cl); 278 m, ν_2(Cu–Cl) cm^{-1}; ν(aryl–H) probably obscured.

[Cu(Tba)$_2$](ClO$_4$)$_2$ (**18**). From 0.370 g (1 mmol) Cu(ClO$_4$)$_2$·6H$_2$O and 0.272 g (2 mmol) Tba Yield: 0.508 g (0.91 mmol, 91% referred to Cu and Tba) brown platelets. Elemental analysis calculated for C$_8$H$_{16}$Cl$_2$Cu$_1$N$_4$O$_{12}$S$_2$ (558.80): C 17.20, H 2.89, N 10.03; found: C 17.23, H 2.88, N 10.03%. IR (KBr pellet): 3428 s, ν_{as}(N–H); 3329 s, ν_s(N–H); 2975 s, 2927 w, ν(C–H); 1653 s, 1600 m, ν(C=O), ν(NH$_2$); 1388 m, ν(C–N); 1086 vs, 580 s, ClO$_4^-$; 575 m, δ(N–C=O); 623 m, ν(S–C) cm^{-1}.

3.4.3. Further Syntheses

[Cu(Ina)$_2$(H$_2$O)$_3$(SiF$_6$)]·H$_2$O (**4**). Amounts of 173 mg (0.5 mmol) Cu(BF$_4$)$_2$·6H$_2$O and 62 mg (0.5 mmol) Ina were each dissolved in 15 mL EtOH, stirred at 70 °C for 30 min and then the two solutions were combined. Standing for about 2 weeks in a glass beaker while letting the solvent evaporate allowed collecting blue needles. Yield: 0.104 g (0.2 mmol, 40% referred to Cu and 80% to Ina). Elemental analysis calculated for C$_{12}$H$_{20}$Cu$_1$F$_6$N$_4$O$_6$Si$_1$ (521.94): C 27.61, H 3.86, N 10.73; found: C 27.63, H 3.86, N 10.74%. IR (KBr pellet): 3695-3270 m, ν(O–H) H$_2$O; 3423 s, 3316 s, ν_{as}(N–H); 3181 s, ν_s(N–H); 3079 m, ν(pyr–H); 1705 s, ν(C=O); 1626 m, δ(NH$_2$); 1612 s, 1552 s, ν(C=C), ν(C=N); 1421 s, ν(C–C); 1388 s, ν(C–N); 740 s, SiF$_6^{2-}$; 490 s, δ(N–C=O) cm^{-1}. FIR (KBr pellet) 286 m, ν(Cu–N); 255 m, ν(Cu–N); 186 m, ν(Cu–F) cm^{-1}.

[Cu(Ina)$_2$Br$_2$] (**5**) was synthesised by dissolving 216 mg (0.5 mmol) [Cu(Ina)$_2$(NO$_3$)$_2$] (**2**) and 71 mg (0.6 mmol) KBr each in 30 mL of EtOH at 70 °C. Mixing of the two solutions produced a green precipitate which was filtered off and dissolved in 20 mL of water. Slow evaporation gave 58 mg (0.125 mmol, 25%) green needles after about 3 weeks. Elemental analysis calculated for C$_{12}$H$_{12}$Cu$_1$Br$_2$N$_4$O$_2$ (467.61): C 30.82, H 2.59, N 11.98; found: C 30.83, H 2.56, N 11.94%. IR (KBr pellet): 3402 s, 3248 m, ν_{as}(NH$_2$); 3186 s, ν_s(NH$_2$); 3067 m, ν(pyr–H); 1714 s, ν(C=O); 1661 s, δ(NH$_2$); 1609 s, 1556 m, ν(C=C), ν(C=N); 1416 s, ν(C–C); 1118 w, ν(CN); 546 s, δ(N–C=O) cm^{-1}. Qualitatively, the compound can also be prepared by grinding [Cu(Ina)$_2$(NO$_3$)$_2$] (**2**) with KBr in a mortar. The compound was previously reported [39] but no details as to the Cu:ligand ratio were provided.

(HIna)$_2$[CuCl$_4$]·2H$_2$O (**6**). Amounts of 85.5 mg (0.5 mmol) CuCl$_2$·2H$_2$O and 61 mg (0.5 mmol) Ina were dissolved in EtOH and 1.3 mL concentrated HCl were added. The mixture was heated up to 70 °C and then left for slow evaporation of the solvent at ambient temperatures in the fume hood. After about 20 days, 126 mg (0.26 mmol, 52%) of blue plates were obtained. Elemental analysis calculated for C$_{12}$H$_{18}$Cl$_4$Cu$_1$N$_4$O$_4$ (487.64): C 29.56, H 3.72, N 11.49; found: C 29.55, H 3.70, N 11.50%.

(HIna)[Cu(H$_2$O)Cl$_3$] (**7**). Amounts of 85.5 mg (0.5 mmol) CuCl$_2$·2H$_2$O and 61 mg (0.5 mmol) Ina were suspended in 12 mL H$_2$O in a Teflon container and 3.5 mg (0.01 mmol) Gd$_2$O$_3$ and 1.3 mL concentrated HCl were added. The container was heated in an autoclave for 2 days at 140 °C. After cooling and opening the reaction mixture was immersed in a glass beaker. After 4 weeks evaporation, 53 mg (0.17 mmol, 34%) of light blue platelets were obtained. Elemental analysis calculated for C$_6$H$_9$Cl$_3$Cu$_1$N$_2$O$_2$ (311.05): C 23.17, H 2.92, N 9.01; found: C 23.13, H 2.96, N 9.00%. Remark: the role of Gd$_2$O$_3$ as catalyst was checked by a blind reaction without Gd$_2$O$_3$. The reaction occurred very slowly and only traces of the target product were obtained.

4. Conclusions

New Cu^{II} complexes and coordination polymers of isonicotineamide (Ina) and picolinamide (Pia), pyrazine 2-amide (Pya), 2- and 4-amino benzamides (2-Aba and 4-Aba) ligands were synthesised from various Cu^{II} sources. Under the criterion of crystallinity and phase purity we were able to reliably reproduce many of the materials in reasonable yields. Crystal and molecular structures from single-crystal XRD were obtained for all new compounds; phase purity was checked using powder XRD. For the optimisation of the reaction protocols, the Cu:ligand stoichiometry of the starting materials was varied and we observed marked deviations of the Cu:ligand ratio in products compared with the starting materials. For three compounds containing the pyridine amides Ina and Pia, high Cu

loadings of 2:1 were necessary to obtain phase pure compounds with Cu:ligand ratios of 1:4 and 1:2. In contrast to this, for the amino benzamide 4-Aba the optimum ratio of starting materials was 1:3 or 1:2 to obtain compounds with a Cu:ligand ratio of 1:2. In the structures, we exclusively observed O_{amide} and not NH_{2amide} binding to Cu^{II}, in most of the cases supported by chelating of the second N binding function (pyridine, pyrazine, or aminophenyl) on the ligands. The ditopic ligands Ina, Pya, and 4-Aba frequently bridge μ-*O,N* between Cu^{II} centres forming 1D or 2D coordination polymers. Again, no NH_{2amide} binding occurred. However, the same ligands were also found in terminal non-bridging modes. Nitrate, NO_3^-, is often competing with amide ligand binding and might be one important reason for the saturation of Cu^{II} preventing the μ-*O,N* bridging and formation of polymers. The coordination surrounding Cu^{II} in these structures is dominated by the ubiquitous axial elongated octahedral geometry (OE). The second important coordination polyhedron is the square pyramid (SPy). The occurrence of these two polyhedra cannot be correlated with the polymeric or non-polymeric character of the compounds. The strong pyridine, pyrazine, or aminophenyl-*N* functions dominate the equatorial binding plane. O_{amide} occurs in this plane only in chelates with these N functions. Non-chelated O_{amide} binding to Cu^{II} was found in the axial (weak) position as expected, alongside with other weak ligands such as NO_3^-, EtOH, H_2O, BF_4^-, and the peculiar SiF_6^{2-}. X-band EPR spectra of powder samples revealed various spectral symmetry patterns ranging from axial over rhombic to inverse axial. Although the EPR spectra cannot be unequivocally correlated to the observed geometry of Cu^{II} in the solid state structures, the EPR patterns can help to support assumed structures as shown for the compound [Cu(Ina)$_2$Br$_2$] (Ina = isonicotine amide). As UV-vis absorption spectroscopy and magnetic measurements in the solid can also be reasonably correlated with the surrounding of Cu^{II}, we suggest the combination of EPR, UV-vis spectroscopy, and magnetic measurements to elucidate or support possible structures of Cu^{II} compounds with such ligands if no unequivocal structural information is available.

As we can reliably reproduce some of the presented materials here, we will study the biological properties, for example, the antiproliferative activity of selected compounds, in the near future.

References

1. Riascos-Rodríguez, K.; Marks, S.; Evans, P.G.; Hernández-Rivera, S.P.; Ruiz-Caballero, J.L.; Pinñero, D.; Hernaández-Maldonado, A.J. Lithium Functionalization Promoted by Amide-Containing Ligands of a Cu(pzdc)(pia) Porous Coordination Polymer for CO$_2$ Adsorption Enhancement. *Cryst. Growth Des.* **2020**, *20*, 3898–3912. [CrossRef]

2. Li, F.-C.; Li, X.-L.; Tan, L.-K.; Wang, J.-T.; Yao, W.-Z. Evans–Showell-type polyoxometalate-based metal–organic complexes with novel 3D structures constructed from flexible bis-pyrazine-bis-amide ligands and copper metals: Syntheses, structures, and fluorescence and catalytic properties. *Dalton Trans.* **2019**, *48*, 2160–2169. [CrossRef]

3. Hearne, N.; Turnbull, M.M.; Landee, C.P.; van der Merwe, E.M.; Rademeyer, M. Halide-bi-bridged polymers of amide substituted pyridines and -pyrazines: Polymorphism, structures, thermal stability and magnetism. *CrystEngComm* **2019**, *21*, 1910–1927. [CrossRef]

4. Kumar, S.; Sharma, R.P.; Venugopalan, P.; Ferretti, V.; Tarpin, M.; Sayen, S.; Guillon, E. New copper(II) niflumate complexes with N-donor ligands: Synthesis, characterization and evaluation of anticancer potential against human cell lines. *Inorg. Chim. Acta* **2019**, *488*, 260–268. [CrossRef]

5. Kwiatek, D.; Kubicki, M.; Skokowski, P.; Gruszczyńska, J.; Lis, S.; Hnatejko, Z. Five subsequent new pyridine carboxamides and their complexes with d-electron ions. Synthesis, spectroscopic characterization and magnetic properties. *J. Mol. Struct.* **2019**, *1178*, 669–681. [CrossRef]

6. Kwiatek, D.; Kubicki, M.; Belter, J.; Jastrząb, R.; Wiśniewska, H.; Lis, S.; Hnatejko, Z. Synthesis, spectroscopic characterization and antifungal activity studies of five novel complexes with pyridine carboxamides. *Polyhedron* **2017**, *133*, 187–194. [CrossRef]

7. Nguyen, T.V.; Ong, T.D.; Lam, A.H.M.; Pham, V.T.; Phan, N.T.S.; Truong, T. Nucleophilic trifluormethylation of aryl boronic acid under heterogeneous Cu(INA)$_2$ catalysis at room temperature: The catalytic copper-based protocol. *Mol. Catal.* **2017**, *436*, 60–66. [CrossRef]

8. Chen, Y.; Li, L.; Li, J.; Ouyang, K.; Yang, J. Ammonia capture and flexible transformation of M-2(INA) (M = Cu, Co, Ni, Cd) series materials. *J. Hazard. Mater.* **2016**, *306*, 340–347. [CrossRef]

9. Chen, Y.; Li, L.; Yang, J.; Wang, S.; Li, J. Reversible flexible structural changes in multidimensional MOFs by guest molecules (I$_2$, NH$_3$) and thermal stimulation. *J. Solid Stat. Chem.* **2015**, *226*, 114–119. [CrossRef]

10. Zurowska, B. Structural and magnetic characterization of Cu–picolinate and Cu–quinaldinate and their mixed complexes with water or halides. *Inorg. Chim. Acta* **2014**, *418*, 136–152. [CrossRef]

11. Wang, P.; Li, G.; Chen, Y.; Chen, S.; James, S.L.; Yuan, W. Mechanochemical interconversion between discrete complexes and coordination networks—Formal hydration/dehydration by LAG. *CrystEngComm* **2012**, *14*, 1994–1997. [CrossRef]

12. He, Y.-C.; Yang, J.; Yang, G.-C.; Kan, W.-Q.; Ma, J.-F. Solid-state single-crystal-to-single-crystal transformation from a 2D layer to a 3D framework mediated by lattice iodine release. *Chem. Commun.* **2012**, *48*, 7859–7861. [CrossRef] [PubMed]

13. Lian, T.T.; Chen, S.-M. A new microporous Cu(II)-isonicotinate framework with 8-connected bcu topology. *Inorg. Chem. Commun.* **2012**, *18*, 8–10. [CrossRef]

14. Monfared, H.H.; Vahedpour, M.; Yeganeh, M.M.; Ghorbanloo, M.; Mayer, P.; Janiak, C. Concentration dependent tautomerism in green [Cu(HL^1)(L^2)] and brown [Cu(L^1)(HL^2)] with H$_2$L^1 = (*E*)-*N*′-(2-hydroxy-3-methoxybenzylidene)-benzoylhydrazone and HL^2 = pyridine-4-carboxylic (isonicotinic) acid. *Dalton Trans.* **2011**, *40*, 1286–1294. [CrossRef]

15. Dakovic, M.; Jaglicic, Z.; Kozlevcar, B.; Popovic, Z. Association of copper(II) isonicotinamide moieties via different anionic bridging ligands: Two paths of ferromagnetic interaction in the azide coordination compound. *Polyhedron* **2010**, *29*, 1910–1917. [CrossRef]

16. Dakovic, M.; Popovic, Z. Uncommon isonicotinamide supramolecular synthons in copper(II) complexes directed by nitrate and perchlorate anions. *Acta Cryst.* **2009**, *C65*, m361–m366.

17. Svorec, J.; Lörinc, S.; Moncol, J.; Melnik, M.; Koman, M. Structural and spectroscopic characterization of copper(II) tolfenamate complexes. *Trans. Met. Chem.* **2009**, *34*, 703–710. [CrossRef]

18. Lörinc, S.; Švorec, J.; Melnik, M.; Koman, M. Structure and spectral characterisation of copper(II) meclofenamate complexes. *Polyhedron* **2008**, *27*, 3545–3548. [CrossRef]

19. Kavalírova, J.; Korabik, M.; Stachová, P.; Moncol, J.; Sillanpää, R.; Lis, T.; Miklos, D.; Melník, M.; Mrozinski, J.; Valigura, D. Synthesis, spectral and magnetic properties of two different 2-nitrobenzoatocopper(II) complexes containing *N,N*-diethylnicotinamide. *Polyhedron* **2008**, *27*, 1333–1342. [CrossRef]

20. Moncol, J.; Mudra, M.; Lönnecke, P.; Hewitt, M.; Valko, M.; Morris, H.; Svorec, J.; Melnik, M.; Mazur, M.; Koman, M. Crystal structures and spectroscopic behavior of monomeric, dimeric and polymeric copper(II) chloroacetate adducts with isonicotinamide, *N*-methylnicotinamide and *N,N*-diethylnicotinamide. *Inorg. Chim. Acta* **2007**, *360*, 3213–3225. [CrossRef]

21. Pichon, A.; Lazuen-Garay, A.; James, S.L. Solvent-free synthesis of a microporous metal–organic framework. *CrystEngComm* **2006**, *8*, 211–214. [CrossRef]

22. Atac, A.; Yurdakul, S.; Ide, S. Synthesis and vibrational spectroscopic studies of isonicotinamide metal(II) halide complexes. *J. Mol. Struct.* **2006**, *783*, 79–87. [CrossRef]

23. Li, C.-B.; Liu, B.; Gao, G.-G.; Che, G.-B. Hydrogen bonding and π–π stacking in di-μ-isophthalato-bis[bis(isonicotinamide)copper(II)] trihydrate. *Acta Cryst.* **2005**, *E61*, m1705–m1707.

24. Moncol, J.; Kalinakova, B.; Svorec, J.; Kleinova, M.; Koman, M.; Hudecova, D.; Melnik, M.; Mazur, M.; Valko, M. Spectral properties and bio-activity of copper(II) clofibriates, part III: Crystal structure of Cu(clofibriate)$_2$(2-pyridylmethanol)$_2$, Cu(clofibriate)$_2$(4-pyridylmethanol)$_2$(H$_2$O) dihydrate, and Cu$_2$(clofibriate)$_4$(*N,N*-diethylnicotinamide)$_2$. *Inorg. Chim. Acta* **2004**, *357*, 3211–3222. [CrossRef]

25. Goher, M.A.S.; Mautner, F.A. Spectral and structural characterization of copper(I) halide, nitrate and perchlorate complexes of pyrazine carboxamide (pyza) and X-ray crystal structure of polymeric [Cu(pyza)$_2$I]$_n$ complex. *Polyhedron* **2000**, *19*, 601–606. [CrossRef]

26. Aakeroy, C.B.; Beatty, A.M.; Leinen, D.S.; Lorimer, K.R. Deliberate combination of coordination polymers and hydrogen bonds in a supramolecular design strategy for inorganic/organic hybrid networks. *Chem. Commun.* **2000**, 935–936. [CrossRef]

27. Goher, M.A.S.; Abu-Youssef, M.A.M.; Mautner, F.A. [1]D polymeric copper(II) complexes containing bridging tridentate pyrazinato and terminal chloro or azido anions. Synthesis, spectral, structural and thermal study of [CuCl(pyrazinato)(H$_2$O)]$_n$ and [Cu(N$_3$)(pyrazinato)(H$_2$O)]$_n$ complexes. *Polyhedron* **1998**, *17*, 3305–3314. [CrossRef]

28. Goher, M.A.S.; Al-Salem, N.A.; Mautner, F.A.; Klepp, K.O. A copper(II) azide compound of pyrazinic acid containing a new dinuclear complex anion [Cu$_2$(N$_3$)$_6$]$^{2-}$. Synthesis, spectral and structural study of KCu$_2$(pyrazinato)(N$_3$)$_4$. *Polyhedron* **1997**, *16*, 825–831. [CrossRef]

29. Goher, M.A.S.; Mautner, F.A. New Unexpected Coordination Modes of Azide and Picolinato Anions Acting as Bridging Ligands Between Copper(II) and Sodium or Potassium Ions. Synthesis, Crystal Structures and Spectral Characterizations of [MCu(picolinato)(N$_3$)$_2$]$_n$ (M = Na or K) Complexes. *Polyhedron* **1995**, *14*, 1439–1446. [CrossRef]

30. Goher, M.A.S.; Mautner, F.A. Spectroscopic and Crystal Structure Study of NaCu(Picolinato)$_2$(N$_3$)(H$_2$O)$_2$. A Polymeric Structure Containing Simultaneous Bridging Pentadentate Picolinato Anion and μ(1,3) Azido Ligands Between Copper and Sodium Centred Polyhedra. *Polyhedron* **1994**, *13*, 2149–2155. [CrossRef]

31. Sileo, E.E.; Morando, P.J.; Della Vedova, C.; Blesa, M.A. The Thermal Decomposition of Copper(II) Nicotinate and Isonicotinate. *Thermochim. Acta* **1989**, *138*, 233–239. [CrossRef]

32. Sekizaki, M. The Crystal Structure of Bis(pyrazine-2-carboxamide)copper(II) Perchlorate. *Acta Cryst. B* **1973**, *B29*, 327–331. [CrossRef]

33. Mukherjee, R. *Comprehensive Coordination Chemistry II*; Chap. 6.6; Jon, A., McCleverty, J.A., Meyer, T.J., Eds.; Elsevier: Oxford, UK, 2004; Volume 6, p. 747910.

34. Kaim, W.; Schwederski, B.; Klein, A. *Bioinorganic Chemistry: Inorganic Elements in the Chemistry of Life*, 2nd ed.; Wiley: Chichester, UK, 2013.

35. Kaim, W.; Rall, J. Copper—A "Modern" Bioelement. *Angew. Chem. Int. Ed.* **1996**, *35*, 43–60. [CrossRef]

36. Erxleben, A. Interactions of copper complexes with nucleic acids. *Coord. Chem. Rev.* **2018**, *360*, 92–121. [CrossRef]

37. Girma, K.B.; Lorenz, V.; Blaurock, S.; Edelmann, F.T. Coordination chemistry of acrylamide. *Coord. Chem. Rev.* **2005**, *249*, 1283–1293. [CrossRef]

38. Allan, J.R.; McCloy, B.; Paton, A.D. Preparation, thermal, structural and electrical studies of dichlorohexa(anthranilamide) cobalt(II) and dichloro(anthranilamide) copper(II). *Thermochim. Acta* **1994**, *231*, 121–128. [CrossRef]

39. Ahuja, I.S.; Singh, R.; Rai, C.P. Complexes of Copper(II) with Nicotinic Acid and some Related Ligands. *Trans. Met. Chem.* **1977**, *2*, 257–260. [CrossRef]

40. Damous, M.; Denes, G.; Bouacida, S.; Hamlaoui, M.; Merazig, H.; Darand, J.-C. Di-μ-chlorido-bis[(2-aminobenzamide-$\kappa^2 N^2$,*O*)chloridocopper(II)]. *Acta Cryst. E* **2013**, *E69*, m488. [CrossRef]

41. Pérez, A.L.; Neuman, N.I.; Baggio, R.; Ramos, C.A.; Dalosto, S.D.; Rizzi, A.C.; Brondino, C.D. Exchange interaction between $S = 1/2$ centers bridged by multiple noncovalent interactions: Contribution of the individual chemical pathways to the magnetic coupling. *Polyhedron* **2017**, *123*, 404–410. [CrossRef]

42. Halcrow, M.A. Jahn-Teller Distortions in Transition Metal Compounds, and Their Importance in Functional Molecular and Inorganic Materials. *Chem. Soc. Rev.* **2013**, *42*, 1784–1795. [CrossRef]

43. Klein, A.; Butsch, K.; Elmas, S.; Biewer, C.; Heift, D.; Nitsche, S.; Schlipf, I.; Bertagnolli, H. Oxido-pincer complexes of copper(II)—An EXAFS and EPR study of mono- and binuclear [(pydotH$_2$)CuCl$_2$]$_n$ (n = 1 or 2). *Polyhedron* **2012**, *31*, 649–656. [CrossRef]

44. Thakurta, S.; Roy, P.; Rosair, G.; Gómez-García, C.J.; Garribba, E.; Mitra, S. Ferromagnetic exchange coupling in a new bis(μ-chloro)-bridged copper(II) Schiff base complex: Synthesis, structure, magnetic properties and catalytic oxidation of cycloalkanes. *Polyhedron* **2009**, *28*, 695–702. [CrossRef]

45. Klein, A.; Elmas, S.; Butsch, K. Oxido Pincer Ligands—Exploring the Coordination Chemistry of Bis(hydroxymethyl)pyridine Ligands for the Late Transition Metals. *Eur. J. Inorg. Chem.* **2009**, *2009*, 2271–2281. [CrossRef]

46. Yraola, F.; Albericio, F.; Corbella, M.; Royo, M. [{Cu(pzPh)(Opo)}$_2$(μ-Cl)$_2$]: A new dinuclear copper(II) complex with a chloride bridge and mixed blocking ligands. *Inorg. Chim. Acta* **2008**, *361*, 2455–2461. [CrossRef]

47. Koval, I.A.; Sgobba, M.; Huisman, M.; Lüken, M.; Saint-Aman, E.; Gamez, P.; Krebs, B.; Reedijk, J. A remarkable anion effect on the crystal packing of two analogous copper complexes from a thiophene-containing phenol-based ligand. *Inorg. Chim. Acta* **2006**, *359*, 4071–4078. [CrossRef]

48. Kilner, C.A.; McInnes, E.J.L.; Leech, M.A.; Beddard, G.S.; Howard, J.A.K.; Mabbs, F.E.; Collison, D.; Bridgeman, A.J.; Halcrow, M.A. A crystallographic, EPR and theoretical study of the Jahn–Teller distortion in [CuTp$_2$] (Tp$^-$ = tris{pyrazol-1-yl}hydridoborate). *Dalton Trans.* **2004**, 236–243. [CrossRef] [PubMed]

49. Klein, C.L.; Stevens, E.D.; O'Connor, C.I.; Majeste, R.J.; Trefonas, L.M. Magnetic Properties and Molecular Structure of Copper(II) Complexes of 2,3-Pyrazinedicarboxamide. *Inorg. Chim. Acta* **1983**, *70*, 151–158.

50. Laussmann, T.; Grzesiak, I.; Krest, A.; Stirnat, K.; Meier-Giebing, S.; Ruschewitz, U.; Klein, A. Copper Thiocyanate Complexes and Cocaine—A Case of Black Cocaine. *Drug Test. Anal.* **2015**, *7*, 56–64. [CrossRef]

51. Glowiak, T.; Podgórska, I. X-ray, Spectroscopic and Magnetic Studies of Hexaaquacopper(II) Di(diphenylphosphate) Diglycine. *Inorg. Chim. Acta* **1986**, *125*, 83–88. [CrossRef]

52. Hathaway, B.; Billing, D. The electronic properties and stereochemistry of mono-nuclear complexes of the copper(II) ion. *Coord. Chem. Rev.* **1970**, *5*, 143–207. [CrossRef]

53. Rieger, P.H. *Electron Spin Resonance—Analysis and Interpretation*; RCS Publishing: Cambridge, UK, 2007.

54. Halcrow, M.A.; Kilner, C.A.; Wolowska, J.; McInnes, E.J.L.; Bridgeman, A.J. Temperature dependence of the electronic ground states of two mononuclear, six-coordinate copper(II) centres. *New J. Chem.* **2004**, *28*, 228–233. [CrossRef]

55. Solanki, N.K.; Leech, M.A.; McInnes, E.J.L.; Mabbs, F.E.; Howard, J.A.K.; Kilner, C.A.; Rawson, J.M.; Halcrow, M.A. A crystallographic and EPR study of the fluxional Cu(II) ion in [CuL2][BF4]2 (L = 2,6-dipyrazol-1-ylpyridine). *J. Chem. Soc. Dalton Trans.* **2002**, 1295–1301. [CrossRef]

56. Mirzaei, M.; Lippolis, V.; Aragoni, M.C.; Ghanbari, M.; Shamsipur, M.; Meyer, F.; Demeshko, S.; Pourmortazavi, S.M. Extended structures in copper(II) complexes with 4-hydroxypyridine-2,6-dicarboxylate and pyrimidine derivative ligands: X-ray crystal structure, solution and magnetic studies. *Inorg. Chim. Acta* **2014**, *418*, 126–135. [CrossRef]

57. Sheldrick, G.M. ShelXT—Integrated space-group and crystal-structure determination. *Acta Crystallogr. Sect. A Found. Crystallogr.* **2015**, *71*, 3–8. [CrossRef] [PubMed]

58. Sheldrick, G.M. *SHELXL-2017/1, Program for the Solution of Crystal Structures*; University of Göttingen: Göttingen, Germany, 2017.

59. Sheldrick, G.M. Crystal structure refinement with *SHELXL*. *Acta Crystallogr. Sect. C Struct. Chem.* **2015**, *71*, 3–8. [CrossRef]

60. STOE X-RED. *Data Reduction Program*; Version 1.31/Windows; STOE & Cie: Darmstadt, Germany, 2005.

61. STOE X-SHAPE. *Crystal Optimisation for Numerical Absorption Correction*; Version 1.06/Windows; STOE & Cie: Darmstadt, Germany, 1999.

62. *STOE WinXPOW 1.07*; STOE & Cie GmbH: Darmstadt, Germany, 2000.

63. Williams, T.; Kelley, C.; Lang, R. Gnuplot 4.6—An Interactive Plotting Program. 2012. Available online: http://gnuplot.info/ (accessed on 23 November 2020).